Design, Synthesis and Biological Evaluation of Novel Hybrids Containing Dihydrochalcone as Tyrosinase Inhibitors to Treat Skin Hyperpigmentation

Songtao Xue,[ǂ,#] Zhiwei Li,[†,#] Xiaotong Ze,[ǂ] Xiuyuan Wu,[ǂ] Chen He,[ǂ] Wen Shuai,[ǂ] Maria Marlow,[†] Jian Chen,[Δ] David Scurr,[†,*] Zheying Zhu,[†,*] Jinyi Xu,[ǂ,*] Shengtao Xu[ǂ,Δ,*]

[ǂ]School of Pharmacy, China Pharmaceutical University, 639 Longmian Avenue, Nanjing, 211198, P. R. China

[†]School of Pharmacy, The University of Nottingham, University Park Campus, NG7 2RD, UK.

[Δ]Department of Hepatobiliary Surgery, The First People's Hospital of Kunshan, Suzhou, 215300, P. R. China

Abstract: Excessive melanin deposition may lead to a series of skin disorders. The production of melanin is carried out by melanocytes, in which the enzyme tyrosinase performs a key role. In this work, we identified a series of novel tyrosinase inhibitor hybrids with a dihydrochalcone skeleton and resorcinol structure, which can inhibit tyrosinase activity and reduce the melanin content in the skin. Compound **11c** possessed the most potent activity against tyrosinase, showing IC_{50} values at nanomolar concentration ranges, along with significant antioxidant activity and low cytotoxicity. Furthermore, *in vitro* permeation tests, supported by HPLC analysis and 3D OrbiSIMS imaging visualisation, revealed the excellent permeation of **11c**. More importantly, compound **11c** reduced the melanin content on UV-induced skin pigmentation in a

guinea pig model *in vivo*. These results suggest that compound **11c** may serve as a promising potent tyrosinase inhibitor for the development of a potential therapy to treat skin hyperpigmentation.

INTRODUCTION

Hyperpigmentation is a common skin disorder that results in the localized darkening of the skin due to an increase in melanin.[1] Melanin is an irregular light-absorbing substance produced by melanocytes located in the basal layer of the epidermis.[2] While melanin can protect human skin from excessive ultraviolet radiation (UVR) and environmental pollutants, excessive melanin accumulation can lead to various acute skin disorders such as freckles, sun rash, and chloasma,[3–6] as well as skin cancer[7] and post-inflammatory melanosis.[8] However, as hyperpigmentation such as melasma is functionally reversible, long-term treatment can prevent more severe pigmentation.[9,10]

The pathogenesis of hyperpigmentation is generally thought to be related to genetic background, UV exposure, and altered inbody hormone levels.[11] The current treatment for this type of disorder is generally topical. There are two main objectives of such treatments; one is to inhibit melanin production, and the other is to inhibit melanin transport. Inhibition of melanin production is the most commonly targeted mechanism.

The molecular mechanism for small-molecular compounds to inhibit melanosynthesis usually involves the inhibition of melanocyte inducing transcription factor (MiTF).[12] Melanogenesis is activated through the regulation of several

intracellular signalling pathways, including Wnt/β-catenin pathway,[13] NO pathway,[14] MAPK pathway,[15] PI3K/Akt pathway, cAMP/MiTF-M signaling pathway[16] and MC1R/α pathway.[17] MiTF is an integral regulator of these five major signalling pathways and plays a critical role in the control of gene expression of the enzymes tyrosinase (TYR), tyrosine-related protein 1 (TYRP-1), and tyrosine-related protein 2 (TYRP-2).[12]

Melanin production involves complex synthetic pathways, including a combination of enzymes and chemical catalytic reactions, in which TYR is a key rate-limiting enzyme. TYR is expressed only by melanocytes, where melanin synthesis occurs.[18] As a result, inhibiting TYR can reduce melanin production in cells without toxic side effects.[19]

As shown in Figure 1, during the process of melanin synthesis, the active sites of TYR go through three states: reduced state, oxidation state, and deoxidation state. The main difference between them lies in the oxidation state of the copper ions.[20] In the presence of monophenol oxidase, deoxy TYR (E_{deoxy}) binds with oxygen to form oxidized TYR (E_{oxy}), and then E_{oxy} binds with L-Tyrosine (**1**) to further catalyze the formation of L-Dopa (**2**). In the presence of diphenol oxidase, E_{oxy} loses an oxygen atom to form reduced TYR (E_{met}), and L-Dopa is oxidized into dopaquinone (**3**). Two adjacent copper ions are bridged at the active site by water (hydroxyl) ligands. TYR exists mainly in the form of E_{met}, which cannot oxidize monophenolic compounds (such as L-Tyrosine) and needs to be reduced to E_{deoxy} by L-Dopa before tyrosine oxidation.[19]

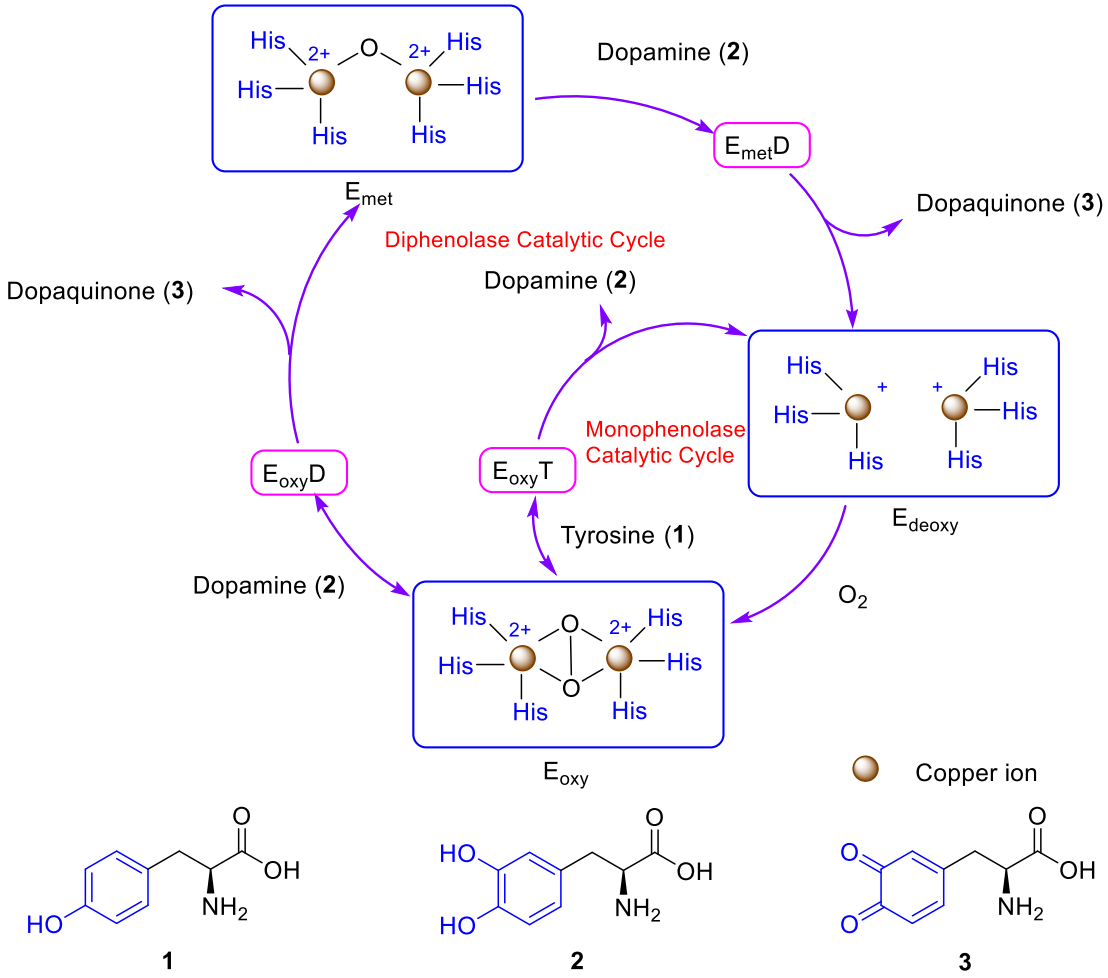

Figure 1. Catalytic cycle of TYR: catalytic cycle of monophenol oxidase and diphenol oxidase. Three types of TYR are E_{oxy}, E_{met}, and E_{deoxy} respectively. $E_{oxy}T$, $E_{oxy}D$, and $E_{met}D$ are E_{oxy}-tyrosine, E_{oxy}-dopamine, and E_{met}-dopamine complexes respectively. Sphere shape represents copper ions with different oxidation states.

Groups of compounds with TYR inhibitory activity have been developed and can be divided into resveratrol analogues,[21–26] phenylthiourea analogues,[27–32] peptides[33–34], and flavonoids.[35–38] Although most of the inhibitors targeting TYR have proven to be effective *in vitro*, only a few are progressed to the clinical stage because of low bioavailability, non-negligible skin irritation, or poor stability. TYR inhibitors such as

hydroquinone (**4**),[39] arbutin (**5**),[40] azelaic acid (**6**),[41] *L*-ascorbic acid (**7**),[42] ellagic acid (**8**),[43] and kojic acid (**9**)[44] have been used clinically and have been shown to reduce skin pigmentation and cure skin disorders (Figure 2). They have been mainly used in cosmetics, with some side effects such as low skin permeation, instability, high cytotoxicity, and carcinogenicity.[45–48] Due to these factors, their applications are limited. Therefore, it is essential to develop more effective new agents with low toxicity and high skin permeability for the treatment of skin hyperpigmentation.

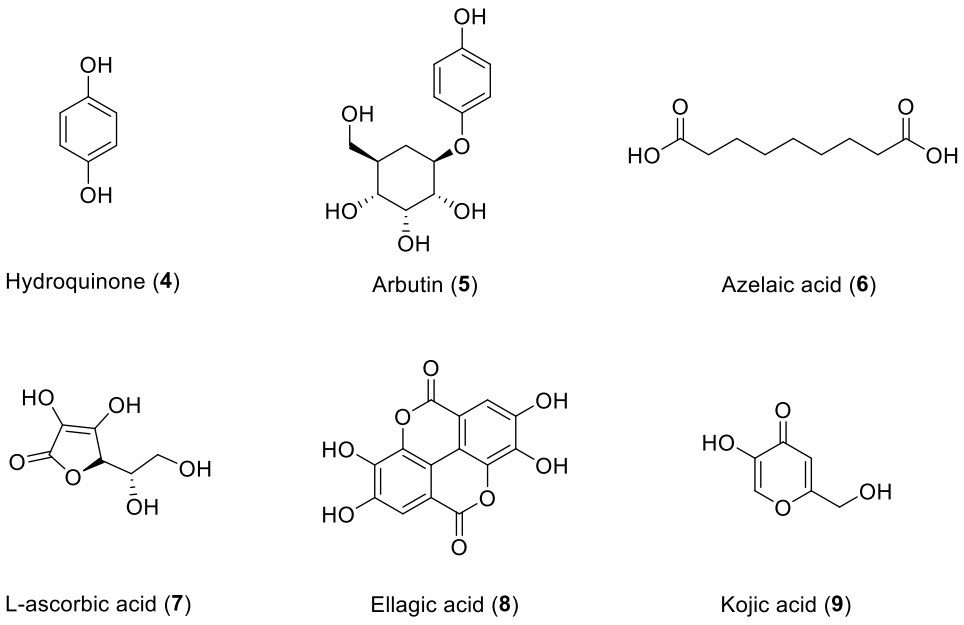

Figure 2. Structures of commercially available TYR inhibitors.

Dihydrochalcone (**10**) compounds belong to a class of compounds called flavonoids with the structural skeleton of 1,3-diphenylacetone.[49] They have a variety of biological activities, i.e., hypoglycemia, antioxidation, anti-tumor, hypopigmentation, and anti-inflammation. In this study, a dihydrochalcone moiety was chosen as the

synthetic backbone, with the goal of designing superior novel tyrosinase inhibitors. As reported previously,[45,46,50,51] resorcinol is the key pharmacophore of TYR inhibitors, and compounds containing this group have good TYR inhibitory activity. In order to obtain more effective tyrosinase inhibitors with better permeability, we designed and synthesized a series of novel dihydrochalcone hybrids by introducing the resorcinol structure into the skeleton of dihydrochalcone (Figure 3) to explore the SAR of TYR inhibitors and identify a novel candidate agent for the potential treatment of skin hyperpigmentation.

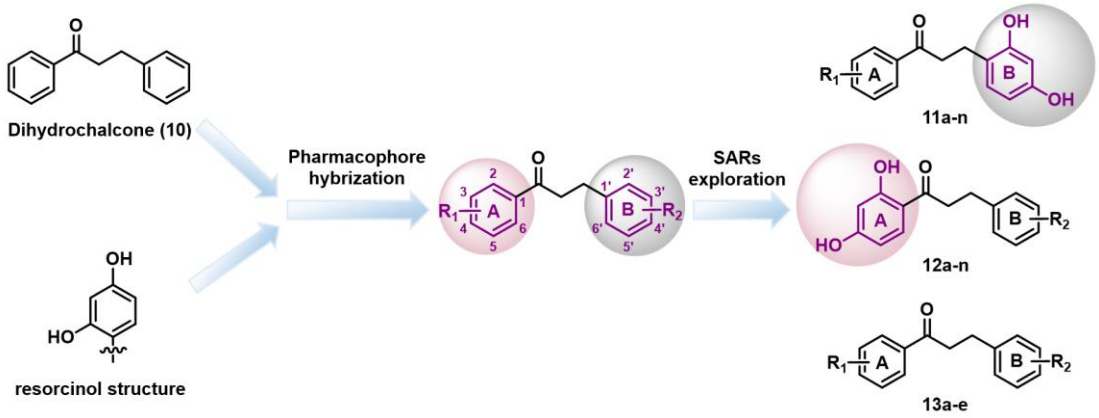

Figure 3. Design strategy of novel dihydrochalcone hybrids as TYR inhibitors.

Hererin, we would like to report the design, synthesis, and biological evaluation of these novel hybrids containing dihydrochalcone and resorcinol moieties. Their activity was assessed in the *in vitro* enzyme and cell models. The most potent compound was selected and assessed comprehensively using High Performance Liquid Chromatography (HPLC) analysis and 3D Orbitrap Secondary Ion Mass Spectrometry

(OrbiSIMS) imaging to visualize and analyze the permeability of the compound. The effect of prophylaxis and repairing was assessed in the guinea pig skin models after topical administration.

RESULTS AND DISCUSSION

Chemistry. As shown in Scheme 1, compounds **11a–n** with ring B containing a resorcinol structure were synthesized. Starting from commercially available 2,4-dihydroxybenzaldehyde (**14**), compound **15** with protected hydroxyl group was obtained by reaction with benzyl bromide. Compounds **16a–n** were prepared by aldol condensation between compound **15** and various acetophenone bearing different substituents, followed by the reduction of the double bond to give compounds **17a–n** in the presence of bis(pinacolato)diboron and catalytic Cs_2CO_3. Finally, in the presence of BCl_3 as a Lewis acid and pentamethylbenzene as an acid-acceptor, the benzyl group was removed to obtain the corresponding target compounds **11a–n**.

Scheme 1. Synthesis of compounds **11a–n**[a]

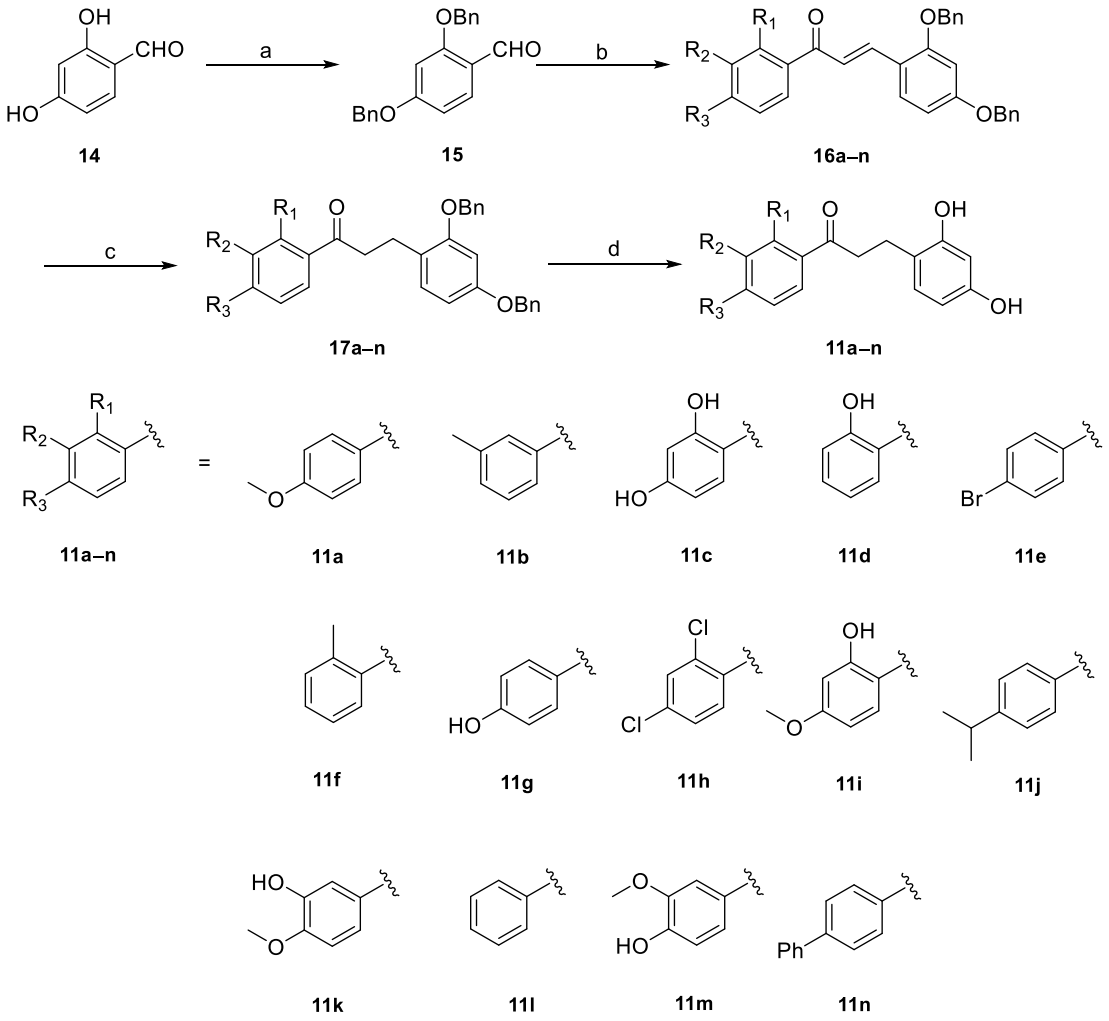

[a]Reagents and conditions: (a) Benzyl bromide, K_2CO_3, MeOH, reflux, 2 h; (b) Various acetophenone, NaOH, EtOH, reflux, 2–4 h; (c) Bis(pinacolato)diboron, Cs_2CO_3, EtOH, sealed tube, 130–150 °C; (d) 1 M BCl_3, dry DCM, - 78 °C or 0 °C, Ar, 20 min.

In order to explore the SAR as well as the significance of the resorcinol structure and the importance of its location for the biological activity, a similar synthetic route was used to obtain compounds **12a–n** (Scheme 2) whose A ring contained a resorcinol structure, in addition to compounds **13a–e** (Scheme 3) whose A ring and B ring did not contain a resorcinol structure.

Scheme 2. Synthesis of compounds **12a–n**[a]

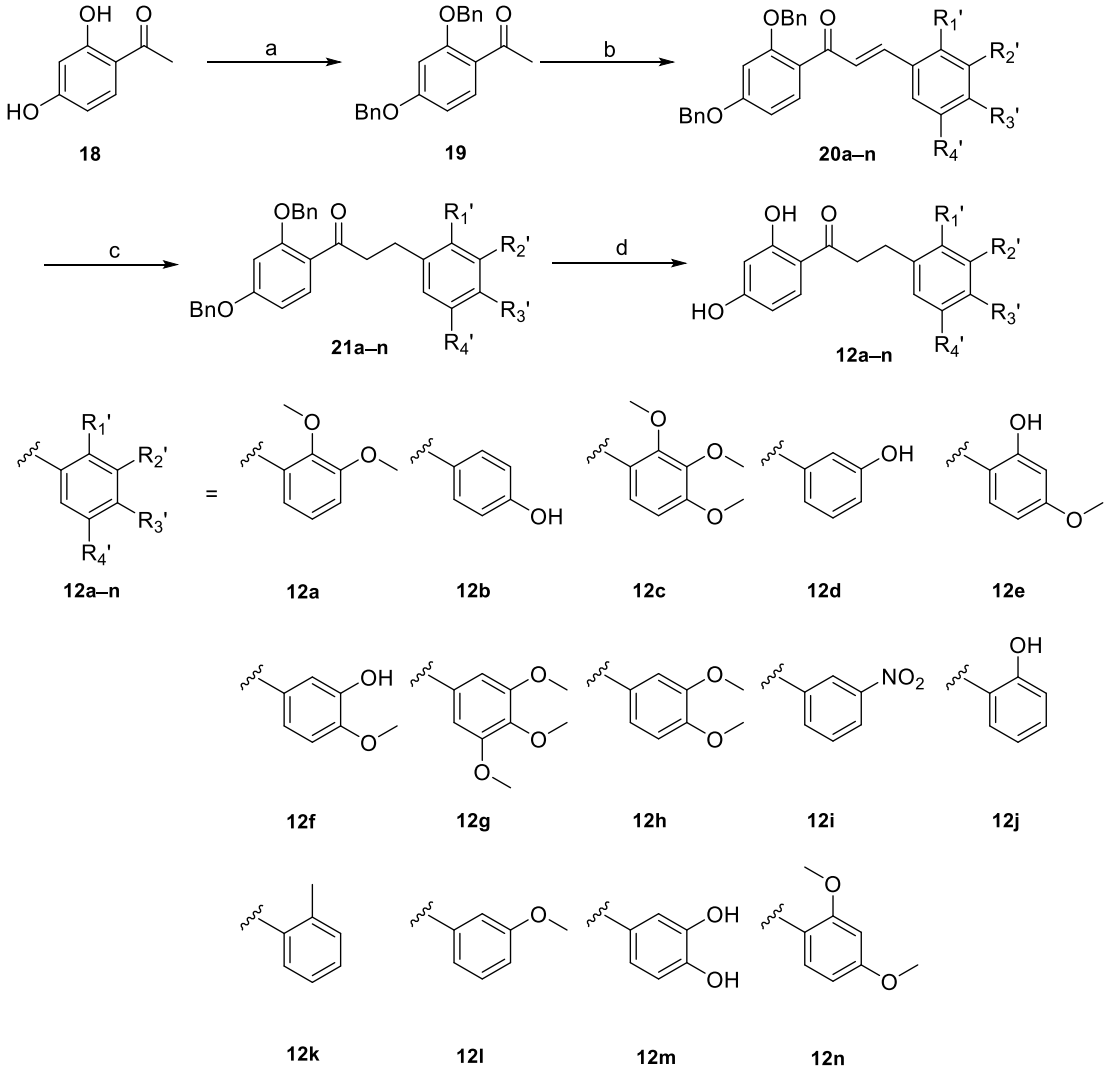

[a]Reagents and conditions: (a) Benzyl bromide, K_2CO_3, MeOH, reflux, 2 h; (b) Various benzaldehyde, NaOH, EtOH, reflux, 2–4 h; (c) Bis(pinacolato)diboron, Cs_2CO_3, EtOH, sealed tube, 130–150 °C; (d) 1 M BCl_3, dry DCM, - 78 °C or 0 °C, Ar, 20 min.

Scheme 3. Synthesis of compounds **13a–e**[a]

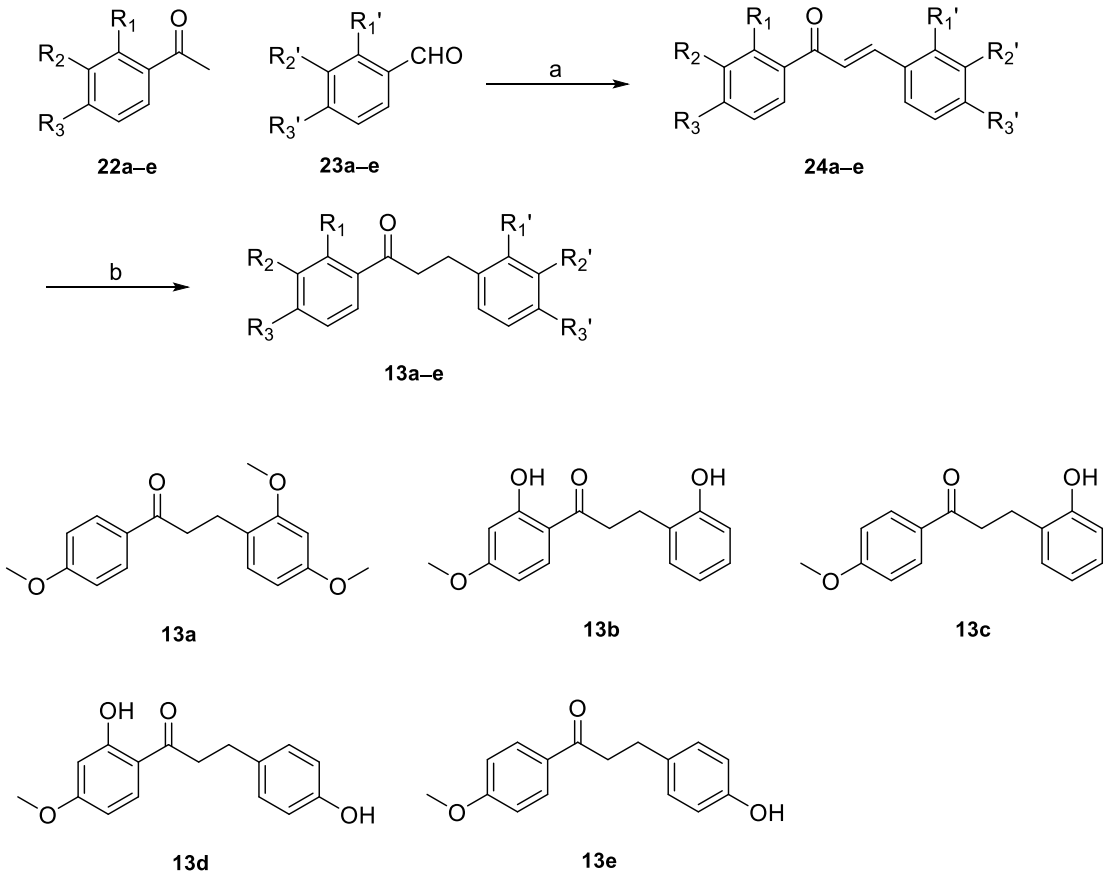

[a]Reagents and conditions: (a) NaOH, EtOH, reflux, 2–4 h; (b) Bis(pinacolato)diboron, Cs_2CO_3, EtOH, sealed tube, 130–150 ℃.

Mushroom TYR inhibitory activity of target compounds. Due to the fact that TYR extracted from *Agaricus bisporus* (mTYR) is pure, stable, and commercially available, it is often used as a model of human TYR to screen TYR inhibitors.[19,34,52] L-Tyrosine and L-Dopa, substrates of monophenol oxidation and diphenol oxidation by TYR, were selected to determine the TYR inhibitory activities of all target compounds by the method reported in the literature.[53]

The results are shown in Table 1. From the results of L-Tyrosine as substrate, it could be seen that when the B ring was a 2',4'-dihydroxyphenyl ring, the mTYR

inhibitory activity of all target compounds was in nanomolar level; when the 2',4'-dihydroxy group on the B ring was replaced with a 3',4'-dihydroxy group (such as **12m**), 2'-hydroxyl group (such as **12j**), or 4'-hydroxyl group (such as **12b**), its inhibitory activity decreased sharply. When the 2',4'-dihydroxy group on the B ring was methylated (such as **12n**), its inhibitory activity was also greatly reduced. These results suggest that a 2',4'-dihydroxyphenyl ring on the B-ring is necessary for mTYR inhibitory activity. Among these compounds, those whose A ring was 2,4-dihydroxyphenyl or 3-methoxy-4-hydroxyphenyl had the best mTYR inhibitory activity, i.e., compound **11c** (L-Tyrosine IC_{50} = 0.050 μM; L-Dopa IC_{50} = 0.064 μM) and **11m** (L-Tyrosine IC_{50} = 0.054 μM; L-Dopa IC_{50} = 0.165 μM). When the substituent on the A ring was 3-hydroxy-4-methoxy (**11k**), its activity decreased slightly (L-Tyrosine IC_{50} = 0.069 μM; L-Dopa IC_{50} = 0.245 μM). When the A ring was substituted by alkyl or halogen groups, its activity decreased, and when the size of alkyl substituents was large, such as 4-phenyl substituted **11n**, its activity decreased significantly. The SAR can be summarized as follows: firstly, the B ring was resorcinol structure and was essential for activity; and secondly, for the A ring, the activity of 2,4-dihydroxyphenyl and 3-methoxy-4-hydroxyphenyl was the best, followed by 2-hydroxy-4-methoxy. The activity would be reduced significantly if substituted by highly hindered alkyl (Figure 4).

Table 1. Inhibitory activity of all target compounds on mTYR.

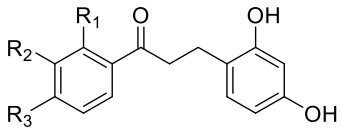

11a–n

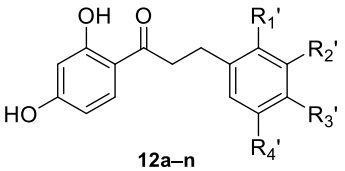

12a–n

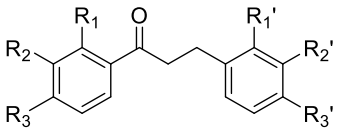

13a–e

Compd.	Structure[a]	IC_{50} (μM)[b]	
		L-Tyrosine	L-Dopa
11a	$R_3 = OCH_3$	0.089 ± 0.008	0.171 ± 0.003
11b	$R_2 = CH_3$	0.133 ± 0.036	0.189 ± 0.008
11c	$R_1 = R_3 = OH$	0.050 ± 0.005	0.064 ± 0.005
11d	$R_1 = OH$	0.069 ± 0.006	0.286 ± 0.028
11e	$R_3 = Br$	0.110 ± 0.010	0.184 ± 0.016
11f	$R_1 = CH_3$	0.123 ± 0.013	0.239 ± 0.018
11g	$R_3 = OH$	0.072 ± 0.017	0.212 ± 0.021
11h	$R_1 = R_3 = Cl$	0.119 ± 0.012	0.189 ± 0.017
11i	$R_1 = OH$; $R_3 = OCH_3$	0.069 ± 0.007	0.183 ± 0.017
11j	$R_3 = CH(CH_3)_2$	0.232 ± 0.024	0.644 ± 0.010
11k	$R_2 = OH$; $R_3 = OCH_3$	0.069 ± 0.007	0.245 ± 0.024
11l	-	0.183 ± 0.016	0.625 ± 0.050
11m	$R_2 = OCH_3$; $R_3 = OH$	0.054 ± 0.005	0.165 ± 0.018
11n	R_3 = phenyl	0.331 ± 0.033	1.431 ± 0.120
12a	$R_1' = R_2' = OCH_3$	> 10	> 10
12b	$R_3' = OH$	> 10	> 10
12c	$R_1' = R_2' = R_3' = OCH_3$	> 10	> 10
12d	$R_2' = OH$	> 10	> 10

12e	R_1' = OH; R_3' = OCH_3	> 10	> 10
12f	R_2' = OH; R_3' = OCH_3	> 10	> 10
12g	R_2' = R_3' = R_4' = OCH_3	> 10	> 10
12h	R_2' = R_3' = OCH_3	> 10	> 10
12i	R_2' = NO_2	> 10	> 10
12j	R_1' = OH	> 10	> 10
12k	R_1' = CH_3	> 10	> 10
12l	R_2' = OCH_3	> 10	> 10
12m	R_2' = R_3' = OH	> 10	> 10
12n	R_1' = R_3' = OCH_3	> 10	> 10
13a	R_3 = R_1' = R_3' = OCH_3	> 10	> 10
13b	R_1 = R_1' = OH; R_3 = OCH_3	> 10	> 10
13c	R_3 = OCH_3; R_1' = OH	> 10	> 10
13d	R_1 = R_3' = OH; R_3 = OCH_3	> 10	> 10
13e	R_3 = OCH_3; R_3' = OH	> 10	> 10
kojic acid		29.7 ± 2.35	48.7 ± 3.85

[a]Not specifically described substituents are hydrogen.

[b]IC_{50} values are expressed as means ± SD (standard error) of at least three independent experiments.

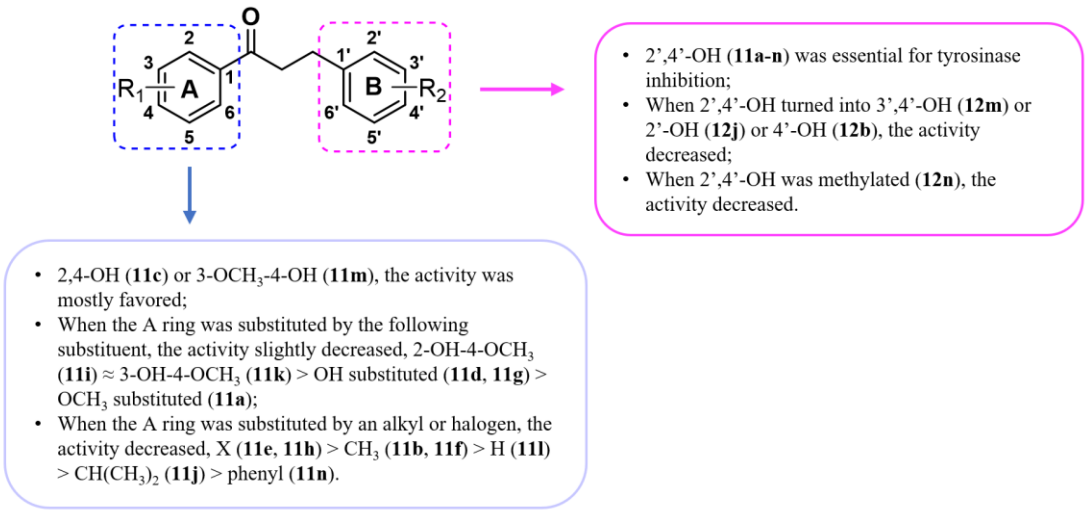

Figure 4. Summary of the structure-activity relationship of dihydrochalcone mTYR inhibitors.

Kinetic studies of mTYR inhibition. Compounds **11c** and **11m** showed the strongest mTYR inhibition, with IC_{50} values of 50 nM and 54 nM respectively. Using Lineweaver Burk double-reciprocal plot, they were selected as representative compounds to analyze mTYR inhibition. The kinetic results of mTYR inhibition in the presence of **11c** and **11m** are shown in Figure 5, which shows four straight lines with 1/V varying with 1/[S], different slopes, and intersecting on the horizontal axis. When the concentration of the compounds was increased, the V_{max} value decreased, while the K_m value remained unchanged, indicating that compounds **11c** and **11m** were non-competitive inhibitors of mTYR, which might exert the inhibitory effect of mTYR by interacting with amino acid residues outside the active center.

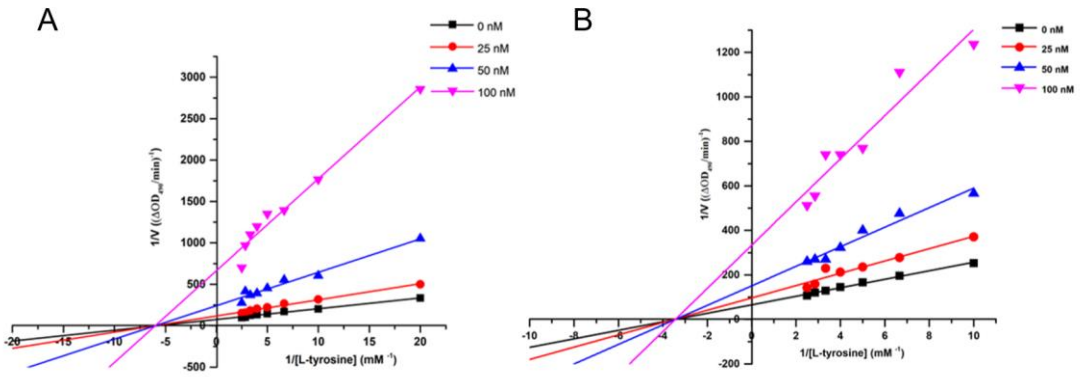

Figure 5. mTYR kinetic characteristic curves of **11c** (A) and **11m** (B).

Molecular docking. We used molecular docking to further explore the mode of interaction of compounds **11c** and **11m** with mTYR. The 3D structure of mTYR used for docking was obtained from *Agaricus bisporus* (PDB ID: 2Y9X). The best docking mode is shown in Figure 6. The B rings of **11c** and **11m** likely occupy the spacious cavity around the active position formed by His61, His85, His259, Asn260, His263, Met280, Gly281, Ser282, Val283, Arg286, Phe292, and two copper ions, whereas the A rings are likely located at the inlet of the active pocket. The 2'-OH group of **11c** appears to form a significant hydrogen bond interaction with Met280, and the B ring likely participates in a π-π stacking interaction with His85, His259, and His263, which further explains the reason why the activity of compounds is greatly reduced when the B ring does not contain the 2',4'-dihydroxy group. The binding mode of the pharmacophore of **11m** and **11c** is similar. Moreover, neither **11c** nor **11m** appears to interact with copper ions. The docking results ulteriorly shows that compounds **11c** and **11m** mainly interact with amino acid residues rather than mTYR active sites and are non-competitive inhibitors.

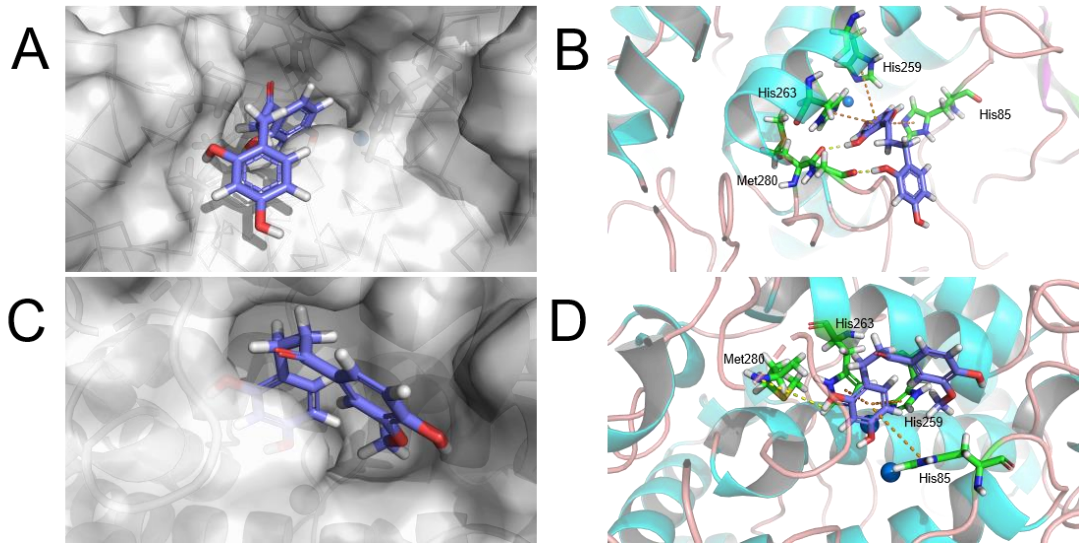

Figure 6. Structures of **11c** (A and B) and **11m** (C and D) bound in the active site of the mTYR from *Agaricus bisporus* (PDB ID: 2Y9X); yellow dashed lines indicate hydrogen bonds; orange dashed lines indicate π–π stacking; blue balls indicate copper ions.

Antioxidant activity of representative compounds 11a–n. Since TYR can catalyze oxidation reactions, antioxidant compounds are capable of inhibiting TYR activity without direct contact with TYR.[54,55] Thus, an assessment of antioxidant activity would help us to further understand the mechanism of compounds inhibiting TYR. 1,1-Diphenyl-2-picrylhydrazyl (DPPH) radical scavenging method was used to evaluate the antioxidant activity of representative compounds **11a–n** at 50 μM, L-ascorbic acid and kojic acid were used as the positive control, and the absorbance at 517 nm was measured by microplate reader. The results in Table 2 show that compounds **11a–n** had gratifying DPPH radical scavenging abilities, which were superior to that of positive control kojic

acid. We speculate that the DPPH radical scavenging effect of compounds **11a–n** was part of its inhibition of melanin production.

Table 2. Antioxidant activity of representative compounds **11a**–**n** at 50 μM.

Compd.	Scavenging activity (%)[a]	Compd.	Scavenging activity (%)[a]
11a	76.56 ± 1.31	**11i**	72.44 ± 0.98
11b	70.50 ± 0.97	**11j**	69.14 ± 1.09
11c	85.47 ± 1.21	**11k**	67.03 ± 0.62
11d	70.98 ± 1.57	**11l**	55.67 ± 0.99
11e	63.36 ± 2.21	**11m**	78.16 ± 1.27
11f	75.85 ± 0.97	**11n**	41.50 ± 0.21
11g	78.72 ± 1.87	kojic acid	28.20 ± 0.58
11h	71.30 ± 0.78	L-ascorbic acid	82.02 ± 2.48

[a]Scavenging activity values are expressed as means ± SD (n = 3).

TYR inhibitory activity of 11c and 11m in murine cell line B16F10. MTT method was used to determine the cytotoxicity of compounds **11c** and **11m** in B16F10 cells at three concentrations (5 μM, 10 μM, and 50 μM). The results are shown in Figure 7A. Even at 50 μM, the cytotoxicity of compounds **11c** and **11m** was minimal compared to the control group.

In order to evaluate the inhibitory effect of the optimal compounds on TYR activity and melanin content in B16F10 melanoma cells, α-Melanocyte stimulating hormone (α-MSH) was used to stimulate B16F10 cells to increase the level of TYR

activity, and then compounds **11c** and **11m** (0, 5, 10 and 25 μM) or positive control (kojic acid, 25 μM) were used to treat B16F10 cells. L-Dopa was used as a substrate for TYR. The results of TYR activity assessment are shown in Figure 7B. Compounds **11c** and **11m** had great inhibitory effects against TYR in cells in a dose-dependent manner and had better TYR inhibitory potential than the positive control kojic acid. Similar to the TYR activity assessment, melanin content in B16F10 cells decreased significantly when treated with increasing concentrations of **11c** and **11m** (Figure 7C).

As reported previously,[56] MiTF is an upstream transcription factor of TYR, which plays an important role in the transcription of the TYR gene. Western blotting demonstrated that the protein levels of both TYR and MiTF in B16F10 cells treated with **11c** decreased in a dose-dependent manner, whereas the inhibition of the protein levels of TYR and MiTF in B16F10 cells treated with kojic acid was relatively weaker compared with that of **11c** (Figure 7D). Altogether, the data indicates that **11c** probably suppresses melanin by both inhibiting the function of TYR and decreasing the TYR content.

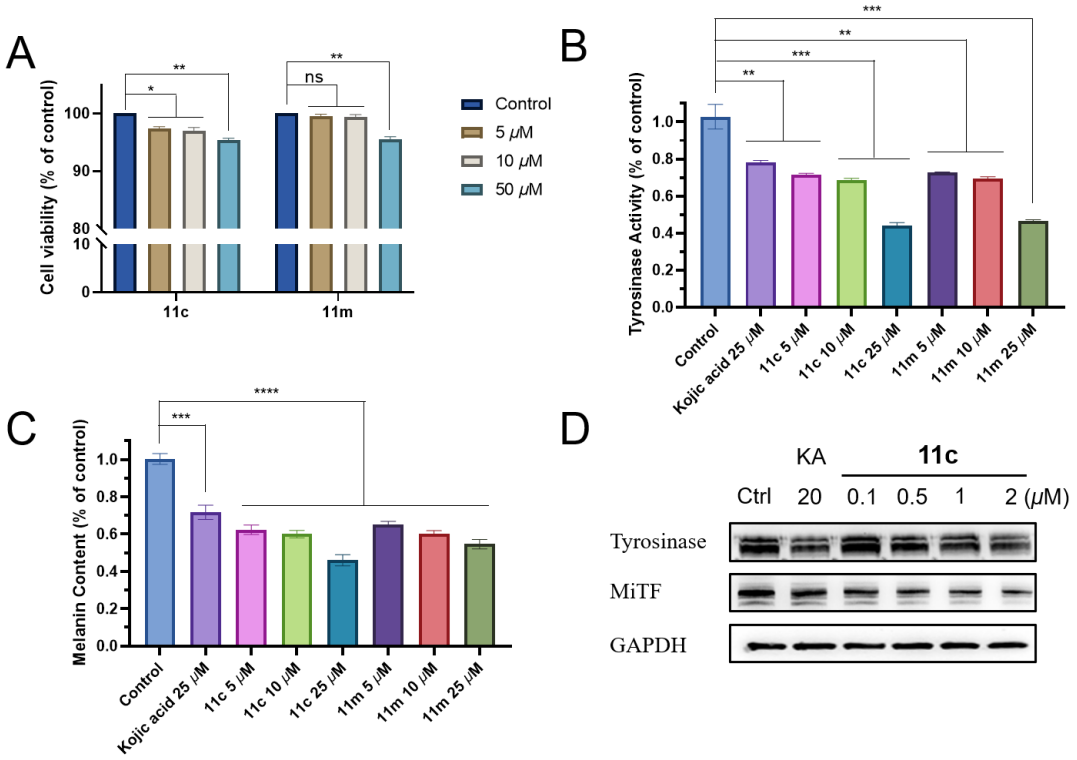

Figure 7. Evaluation in murine cell line B16F10. (A) Cytotoxicity of compounds **11c** and **11m** in B16F10 cells. Inhibitory activities of **11c** and **11m** on TYR (B) and melanin content (C) in B16F10 cells stimulated by α-MSH were tested. The cells were treated with 0, 5, 10, 25 μM of **11c** and **11m** or 25 μM of kojic acid, respectively. The data are expressed as means ± SD (n=3). Statistical significance of differences was assessed using multiple t-test. *, $p < 0.05$; **, $p < 0.01$; ***, $p < 0.001$; ****, $p < 0.0001$. (D) Western blotting. Effects of **11c** and kojic acid on TYR and MiTF levels in B16F10 cells.

TYR inhibitory activity of 11c and 11m in human cells A375. Since the cytotoxicity of **11c** and **11m** was negligible even at a high concentration (50 μM) in murine-derived cells, it is neccessory to verify whether it would be non-toxic in human-derived cells. Therefore, the human malignant melanoma cells A375 were chosen to determine the

cytotoxicity of compounds **11c** and **11m** using the MTT assay, and kojic acid as a positive control. The results are shown in Figure 8A. At a concentration of 50 μM, the cytotoxicity of compound **11m** was negligible compared to the control, while **11c** was slightly cytotoxic.

To ensure that the novel compounds had the same ability to inhibit melanin and TYR activity for human-derived cells, A375 cells were stimulated with α-MSH to increase the level of TYR activity. Then, A375 cells were treated with 20 μM of compounds **11c**, **11m**, and the positive control (kojic acid). The resulting TYR activity and melanin content results are shown in Figures 8B and 8C. Compounds **11c** and **11m** at 20 μM both had a significant inhibitory effect on TYR in A375 cells with a similar capacity to the positive control. Of these, **11c** was slightly superior to **11m**. Similar to the assessment of TYR activity, melanin content in A375 cells was remarkably reduced with the treatment of **11c** and **11m** at 20 μM.

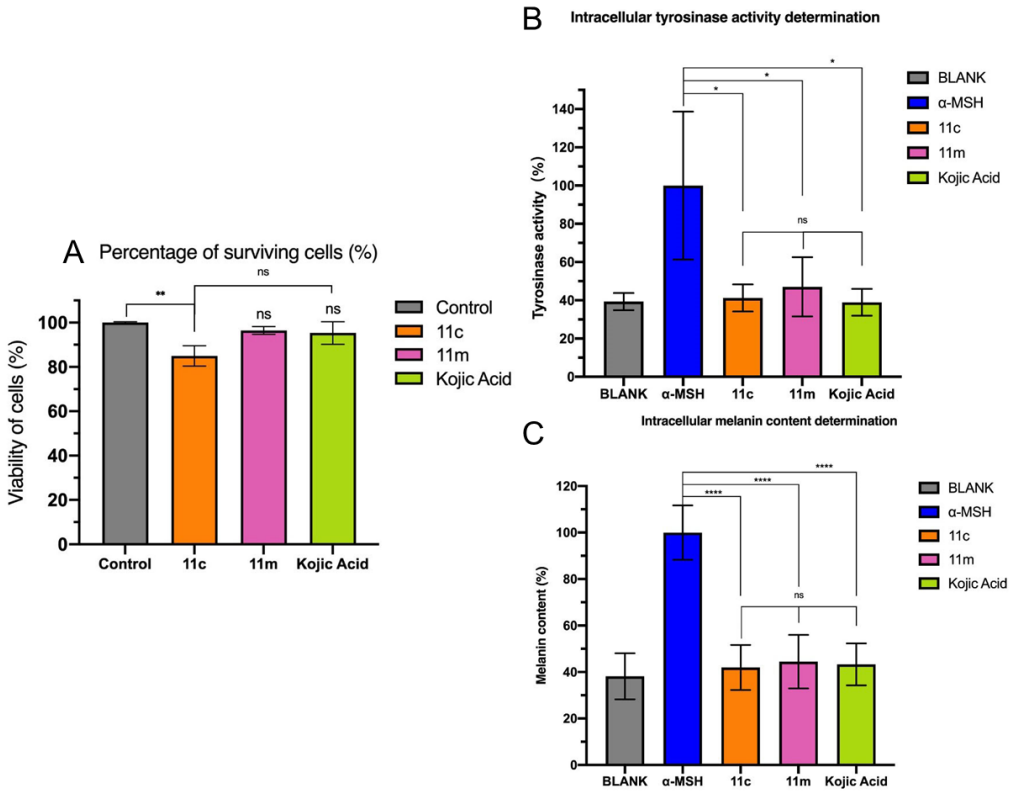

Figure 8. Evaluation in human A375 cells. (A) Cytotoxicity of compounds **11c**, **11m**, and kojic acid in A375 cells. Inhibitory activity of **11c** and **11m** on TYR (B) and melanin content (C) in A375 cells stimulated by α-MSH were tested. The cells were exposed to 20 μM of **11c**, **11m**, and kojic acid for 24 h. Statistical significance of differences was assessed using ANOVA one-way test. (A) Values were significantly different from those of the control group. (n=3, values are means ± SE). (B, C) Values were significantly different from those of the α-MSH group. (B, n=4, C, n=3, values are means ± SE)*, $p < 0.05$; **, $p < 0.01$; ****, $p < 0.0001$.

***In vitro* skin permeation efficiency of compound 11c by Franz cell component.** The skin permeation of **11c** was determined by HPLC analytical methods. Calibration curves and limits of detection and quantification for **11c** and kojic acid were firstly

established according to the chromatographic conditions set up in the Experimental section.

The optimal compound **11c** was then assessed for its skin permeation studies by using the Franz diffusion cell. 2 mg/mL of **11c** in propylene glycol (PG) was used, and 2 mg/mL of kojic acid was chosen as a positive control. The highest skin permeation of **11c** was observed at 2 hours after application, with 26.77% remaining inside the skin (intradermal). In contrast, kojic acid reached its highest level at 4 hours after application, with only 3.56% of the active ingredient remaining in the skin (Figure 9A). In addition, it can be seen from Figures 9B-F that from 0.5 h to 24 h, the amount of **11c** penetrated into receptor fluid (transdermal) was tiny, and the highest level (Figure 9F) didn't exceed 1.2%. Overall, based on the skin permeation studies, the intradermal delivering capacity of **11c** was shown to be superior and far exceeded that of kojic acid. In addition, only a tiny amount of **11c** would be able to enter the circulatory system after transdermal permeation, helping to avoid toxic side effects.

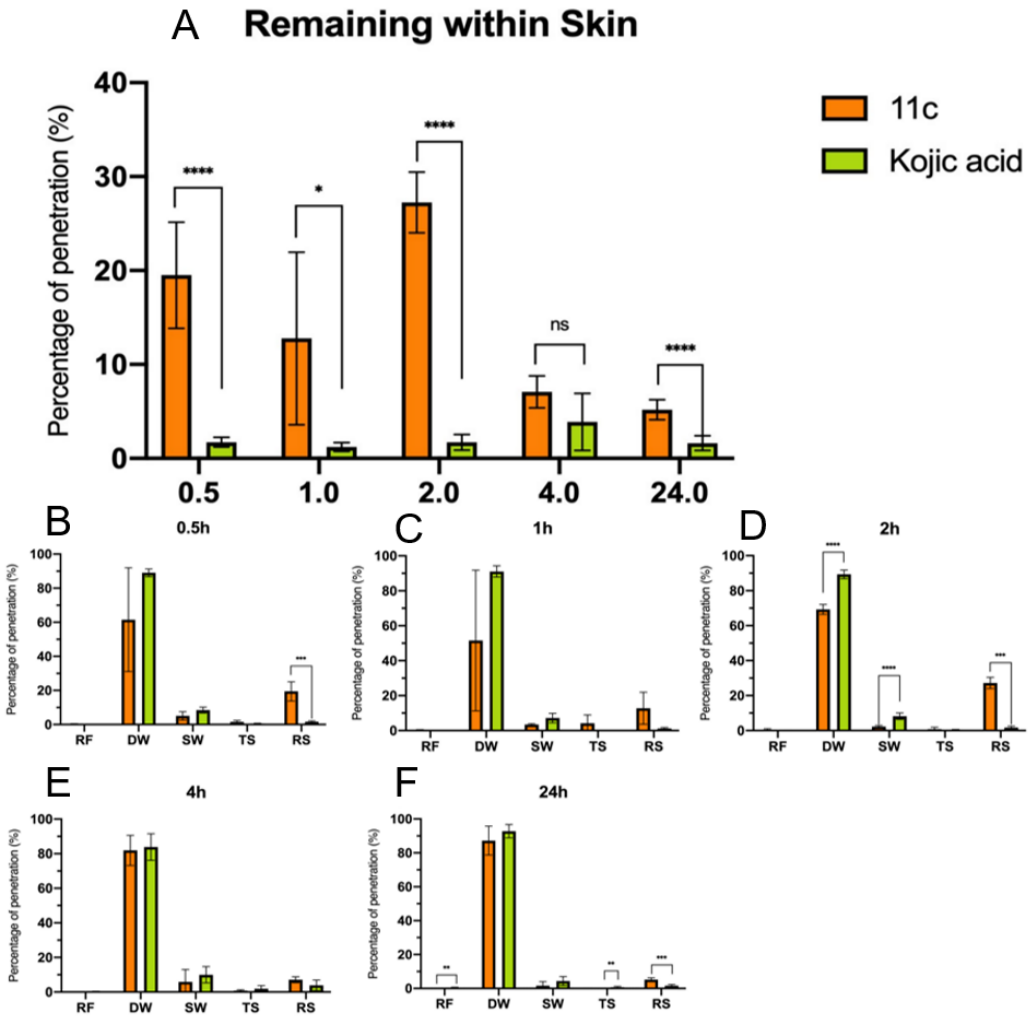

Figure 9. HPLC analysis of the mean percentage of permeation of **11c** in different Franz cell components (donor wash (DW), skin wash (SW), tape strips (TS), remaining within skin (RS), and receptor fluid (RF)) following permeation test at different hours ((B) 0.5h, (C) 1h, (D) 2h, (E) 4h, (F) 24h). (A) The percentage of **11c** remaining within skin (intradermal) at different hours. The data are expressed as means ± SD (n=6). Statistical significance of differences was assessed using multiple t-test (*, $p < 0.05$; **, $p < 0.01$; ***, $p < 0.001$; ****, $p < 0.0001$; no significant difference (ns) indicates $p > 0.05$).

Visualization of compound 11c within the skin by OrbiSIMS. Firstly, according to haematoxylin and eosin (H&E) staining (Figure 10A), the thickness of the stratum corneum is approximately 5-10 μm and the thickness of the epidermis 20-100 μm. The melanocytes containing tyrosinase are located in the basal layer, between the epidermis and dermis, and therefore should be located 100-110 μm from the skin surface.

According to the study of Nichola and co-workers,[57] palmitic acid ($C_{16}H_{31}O_2^-$) can be used to locate the stratum corneum. Cholesterol sulfate ($C_{27}H_{45}SO_4^-$) is then used as an adjunct to locate the uppermost layer of epidermis. The white dashed line in Figure 11A indicates the boundary between the stratum corneum and epidermis. The ion signal of **11c** clearly appeared below the stratum corneum and was distributed in the epidermis. The signal ions of **11c** are mainly $C_{15}H_{13}O_5^-$ and $C_{15}H_{12}O_5Na^-$, as shown in Figure 10B, c-d. The ion $C_{15}H_{13}O_5^-$ resided more in the stratum corneum, and lost a hydrogen ion and was bound to a sodium ion when **11c** entered the epidermis. In addition, identification of the site of penetration of the compound was supported by the fact that the phospholipid marker (PO_3^-) would appear in the epidermis and upper dermis[58] (Figure 10C, f). As shown in Figure 11B, the distance of the green part of the **11c** ion from the skin surface is about 50-150 μm. This indicates that **11c** entered the skin and mainly stayed at the base of the epidermis and in the upper dermis. Thus, it is suggested that compound **11c** targets melanocytes in the basal layer adequately.

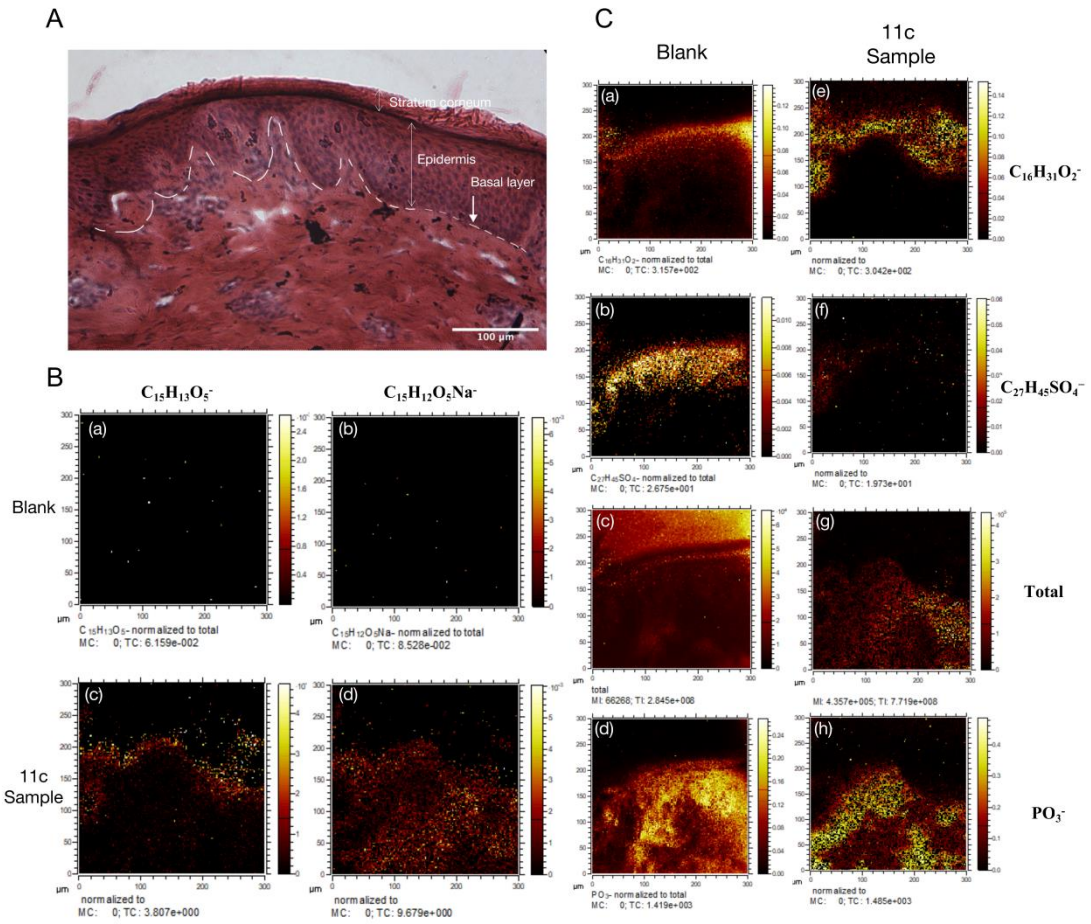

Figure 10. (A) HE-stained cross-section of dermatomed porcine skin (4 mm thick) dosed with **11c** at 2 mg/mL. The basal layer of epidermis is located above the white dashed line (the position indicated by the arrow). Image from 20 μm cryocut tissue section at a 10-fold magnification. (B & C) Negative polarity ion images of 3D OrbiSIMS from various fragment ions of the skin cross section dosed by compound **11c** at 2 mg/mL in dermatomed porcine skin (4 mm thickness), and use water as blank group. The field of view is 300.0 μm and pixelsize is 2.0 μm, MC maximum ion count per pixel and TC total ion count for the specific ion of interest. (B) The ion images illustrate the 2D spatial distribution for the molecular ions of **11c**: (a) **11c** ($C_{15}H_{13}O_5^-$) in blank group; (b) **11c** ($C_{15}H_{12}O_5Na^-$) in blank group; (c) **11c** ($C_{15}H_{13}O_5^-$) in **11c** group; (d) **11c** ($C_{15}H_{12}O_5Na^-$) in **11c** group. All ion images have been normalized to the total ion image. (C) The ion images

illustrate the 2D spatial distribution for the following molecular ions: (a)&(e) palmitic acid ($C_{16}H_{31}O_2^-$); (b)&(f) cholesterol sulfate ($C_{27}H_{45}SO_4^-$); (c)&(g) Total ion; (d)&(h) phospholipid marker (PO_3^-). And (a)-(d) in blank group and (e)-(h) in **11c** group. All ion images have been normalized to the total ion image.

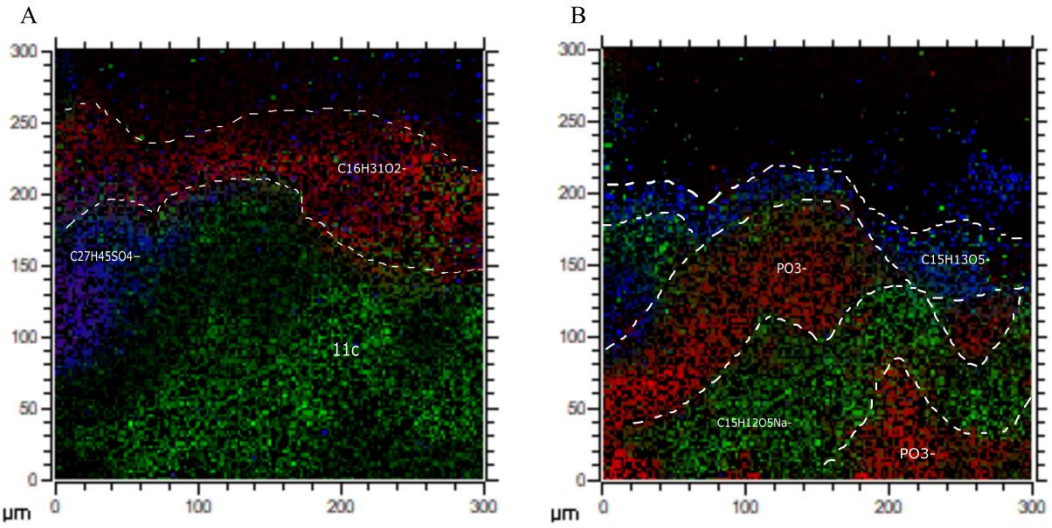

Figure 11. Images of 3D OrbiSIMS from various fragment ions of the skin cross section dosed by 2 mg/mL of **11c** in dermatomed porcine skin (4 mm thickness). The Field of View: 300.0 μm and Pixelsize: 2.0 μm. The ion images illustrate the 2D spatial distribution for the overlay of different molecular ions. (A) Three color overlay between ion images, Stratum corneum, SC (palmitic acid fragment, $C_{16}H_{31}O_2^-$, red), top of epidermis (cholesterol sulfate fragment, $C_{27}H_{45}SO_4^-$, blue) and **11c** ($C_{15}H_{13}O_5^-$, and $C_{15}H_{12}O_5Na^-$, green). (B) Three color overlay between ion images, **11c** ($C_{15}H_{13}O_5^-$, blue), **11c** ($C_{15}H_{12}O_5Na^-$, green), epidermis (phospholipid marker, PO_3^-, red).

***In vivo* treatment of 11c on UV-induced skin pigmentation in a guinea pig model.** Two different methods were applied to evaluate the *in vivo* anti-melanin effect of **11c** in UV-induced skin pigmentation in a guinea pig model. One method was as a prophylactic (Figure 12A) and the other as a treatment for repair (Figure 13A), that is, topical administration of the compound **11c** 6 h before UV radiation every day for 2 weeks, or after exposure to UV lamp for 5 days/week for two consecutive weeks.

Daily topical administration of **11c** inhibited the production of melanin in a dose-dependent manner (Figure 12B). As shown in Figures 12C and 12D, the proportion of cells positive to the Fontana-Masson stain of the skin treated with 0.5 mM **11c** in PG was higher than that of 1 mM **11c** in PG. Different solvents of **11c** had no significant effect on the inhibition of melanin, and duplicate concentration of **11c** in PG and carbomer (CP) hydrogel both reduced the melanin level.

In the batch of repair experiments, compound **11c** in different formulations was applied after receiving UV radiation for 2 weeks. Similar conclusions could be drawn that **11c** was able to heal the scorching skin in a dose-dependent manner, and various solvents had limited influence on the experimental results (Figures 13B, 13C and 13D).

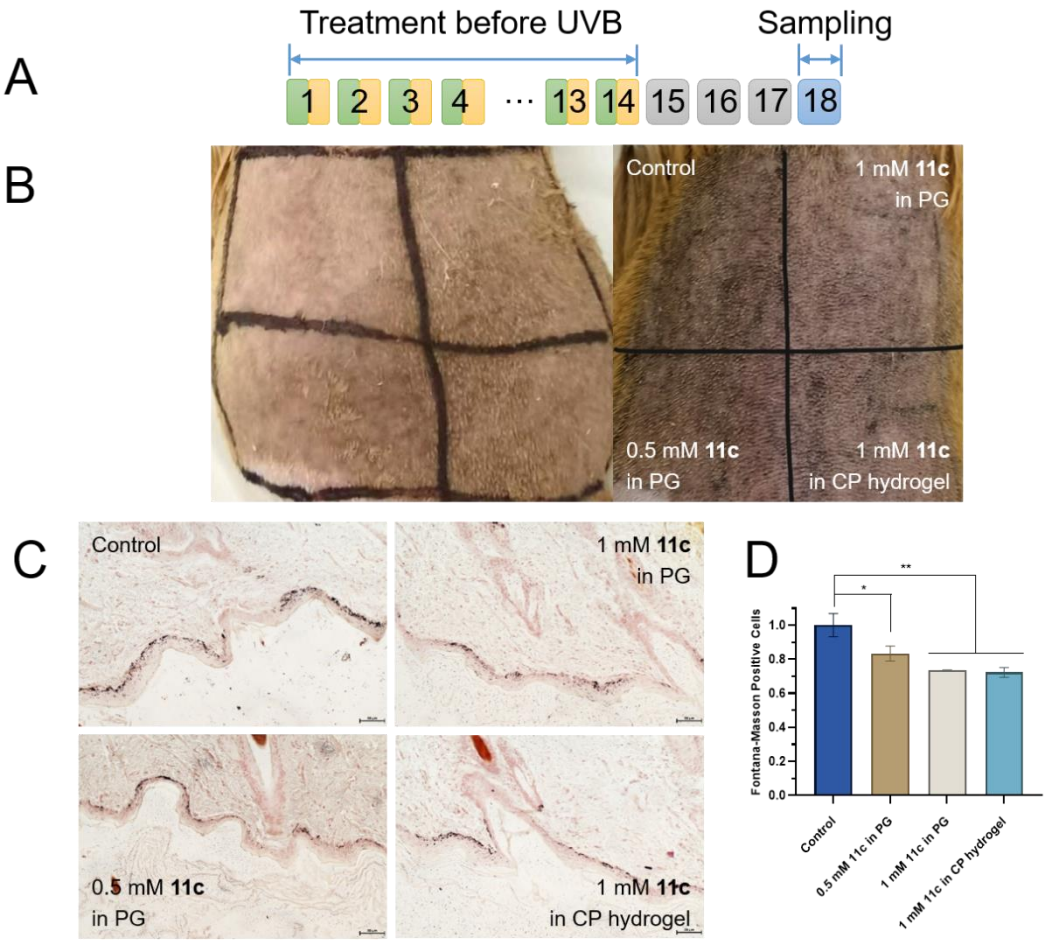

Figure 12. Prophylactic effect of **11c** on UV-induced pigmentation in guinea pig skin. (A) Time schedule of UV irradiation and application of **11c**. (B) Images of the back of guinea pigs before (left) and after (right) UV irradiation. (C) Biopsy specimens were taken from each of the four-square areas of the right guinea pig and silver-stained with a Fontana-Masson staining kit. Bars = 50 μM. (D) Statistics of cells positive for Fontana-Masson stain. The proportion of the positive cells was the ratio of positive cells to the number of epidermal cells in the same visual field with 10 different images for each skin sample. Statistical significance of differences was assessed using multiple t-test. *, $p < 0.05$; **, $p < 0.01$.

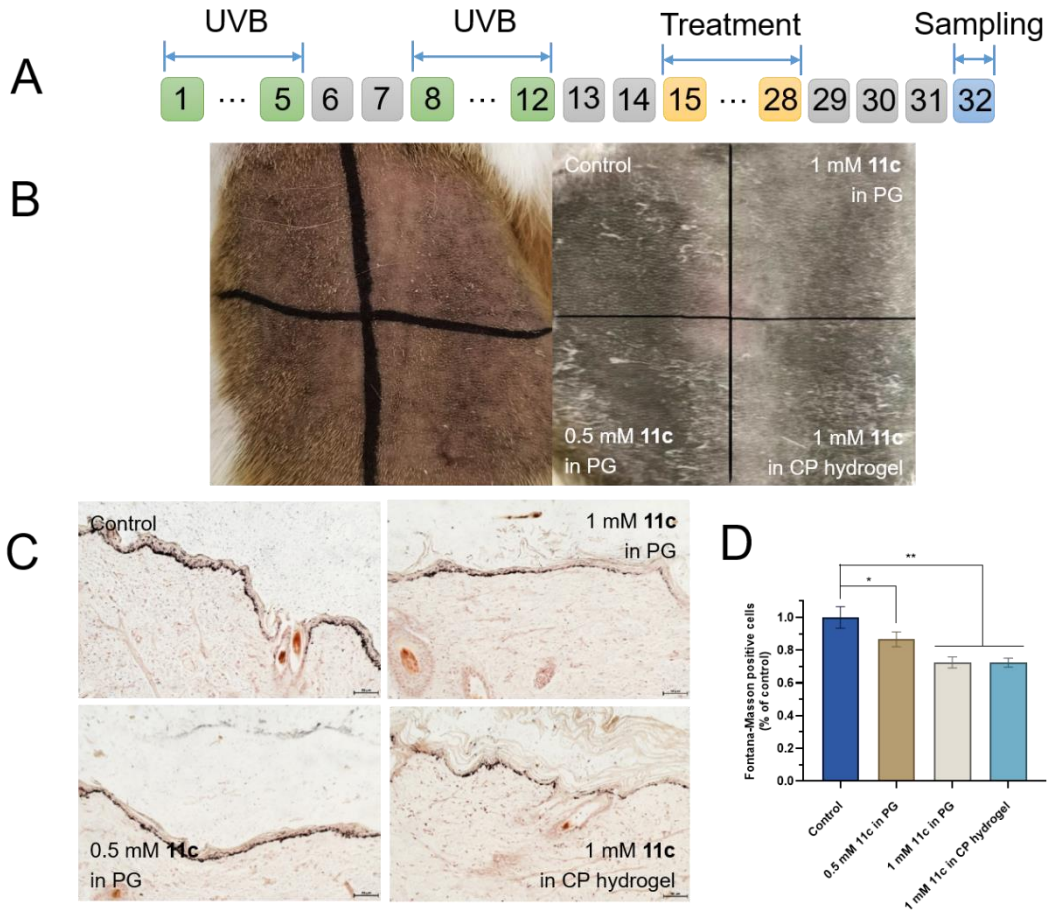

Figure 13. Ability of **11c** to repair UV-induced pigmentation in guinea pig skin. (A) Time schedule of UV irradiation and application of **11c**. (B) Images of the back of guinea pigs after UV irradiation (left) and after UV irradiation and treatment (right). (C) Biopsy specimens were taken from each of the four-square areas of the right guinea pig and silver-stained with a Fontana-Masson staining kit. Bars = 50 μM. (D) Statistics of cells positive for Fontana-Masson stain. The proportion of the positive cells was the ratio of positive cells to the number of epidermal cells in the same visual field with 10 different images for each skin samples. Statistical significance of differences was assessed using multiple t-test. *, $p < 0.05$; **, $p < 0.01$.

CONCLUSIONS

As a key rate-limiting enzyme in the process of melanin formation, TYR has become a target for the inhibition of melanin production. In this study, by applying the pharmacophore fusion strategy, the resorcinol structure was introduced into the skeleton of dihydrochalcone to discover novel TYR inhibitors. Thirty-three dihydrochalcone TYR inhibitors were designed and synthesized, and the mTYR activity of all compounds was evaluated. The mTYR inhibitory activity of fourteen compounds was found to be stronger than that of positive control kojic acid, and the IC_{50} values reached nanomolar levels. Compounds **11c** and **11m** showed the most potent mTYR inhibitory activity with IC_{50} values of 0.050 μM and 0.054 μM respectively (when the substrate was L-Tyrosine). Mechanistic validation experiments showed that **11c** likely suppresses melanin production by inhibiting the function of TYR in a non-competitive manner and by decreasing TYR contents.

Further experimental results showed that compounds **11c** and **11m** have gratifying antioxidant activity and low cytotoxicity, and inhibit TYR activity and melanin production in murine cell line B16F10 in a dose-dependent manner. In human-derived A375 cells, compounds **11c** and **11m** also showed excellent TYR inhibition and melanin suppression. In addition, compound **11c** also shows outstanding performance in *in vitro* skin permeation assays, rapidly crossing the skin stratum corneum and remaining inside the skin, thus targeting the basal layer and focusing on the melanocytes. More importantly, we found that compound **11c** exhibited powerful anti-melanogenesis ability in a guinea pig model *in vivo*.

Taken together, compound **11c** can be considered as a low cytotoxic and effective TYR inhibitor for further development of new therapeutic options for the treatment of skin hyperpigmentation.

EXPERIMENTAL PROCEDURES

Chemistry. All reagents and solvents were purchased from commercial suppliers without further purification unless otherwise indicated. All reactions were monitored by thin-layer chromatography (TLC) and visualized with UV light or iodine stain. ^{1}H NMR and ^{13}C NMR spectra were recorded on Bruker AV-300 or AV-400 spectrometer. Coupling constants (*J*) were expressed in hertz (Hz). Chemical shifts were reported as parts per million (ppm) relative to an internal solvent reference. The following abbreviations were used in the NMR descriptions: s, singlet; d, doublet; t, triplet; q, quartet; m, multiplet; dd, double doublet; and br, broad peak. High-resolution ESI-MS data were recorded on an Agilent QTOF 6520 mass spectrometer. Purity of screening compounds was evaluated by NMR spectroscopy and HPLC analysis, and electron spray ionization (ESI) was used as an ion source. All compounds had purity ≥ 95% by HPLC (SHIMADZU Labsolutions, UV detection at $\lambda = 254$ nm) analysis on the Agilent C18 column (4.6 × 150 mm, 5 μm) eluting at 1 mL/min of menthol and water (75:25).

*2,4-Bis(benzyloxy)benzaldehyde (**15**).* Compound **14** (1 g, 7.24 mmol), K_2CO_3 (3 g, 21.72 mmol) and benzyl bromide (3.44 mL, 28.96 mmol) were added to methanol. The mixture was heated to reflux for 2 h. Then, methanol was removed in vacuo.

Diluted with EtOAc and water, the biphasic solution was extracted three times with EtOAc. The combined organics were washed with brine, dried over anhydrous Na_2SO_4, and concentrated in vacuo. Purification of the residue by column chromatography with PE/EA (10:1) to give 2,4-bis(benzyloxy)benzaldehyde (**15**, 2.0 g, 6.3 mmol, 87%) as a white solid.

16a–n. Compound **15** (300 mg, 0.94 mmol), various acetophenone (1.05 eq.) and NaOH (188.44 mg, 4.71 mmol) were added to ethanol. The mixture was heated to reflux for 2–4 h. Then, ethanol was removed in vacuo. Diluted with EtOAc and water, the biphasic solution was extracted three times with EtOAc. The combined organics were washed with brine, dried over anhydrous Na_2SO_4, and concentrated in vacuo. Purification of the residue by column chromatography with PE/EA to give the target compounds **16a–n** as a yellow solid or oil with good yields.

17a–n. A pressure vial equipped with a magnetic stirring bar was charged with compounds **16a–n**, bis(pinacolato)diboron (3 eq.), Cs_2CO_3 (0.2 eq.) and ethanol. The vessel was flushed with argon, sealed with a crimp cap, and heated to 120–150 ℃ for 12–24 h. The reaction vessel was removed from the oil bath when the reaction was finished, and cooled to room temperature. The precipitate, if appeared, was collected by filtration onto a sintered-glass funnel, washed with cold ethanol (3 × 50 mL), and dried in vacuo to give the target compounds. Otherwise, ethanol was removed in vacuo. Diluted with EtOAc and water, the biphasic solution was extracted three times with EtOAc. The combined organics were washed with brine, dried over anhydrous Na_2SO_4,

and concentrated in vacuo. Purification of the residue by column chromatography with PE/EA to give the target compounds **17a–n** as a white solid with moderate yield.

11a–n. A two-neck flask was charged with compounds **17a–n**, pentamethylbenzene (1.5 eq. per benzyl to be removed) and dry DCM. Under the protection of Ar at 0 ℃ (the intermediate without methoxyl) or -78 ℃ (the intermediate with methoxyl), 1 M BCl_3 (1.5 eq. per benzyl to be removed) was injected into the flask, the solution turned orange and reacted for 20 min. After the reaction was completed, water was added to quench the reaction. Diluted with EtOAc and water, the biphasic solution was extracted three times with EtOAc. The combined organics were washed with brine, dried over anhydrous Na_2SO_4, and concentrated in vacuo. Purification of the residue by column chromatography with DCM/MeOH to give the target compounds **11a–n** with moderate yields.

*3-(2,4-Dihydroxyphenyl)-1-(4-methoxyphenyl)propan-1-one (**11a**)*. Yield 73%, yellow solid; ^{1}H NMR (300 MHz, $CDCl_3$) δ 8.54 (s, 1H), 7.96 (d, J = 8.5 Hz, 2H), 6.96 (s, 1H), 6.92 (d, J = 9.0 Hz, 2H), 6.53 – 6.45 (m, 1H), 6.39 (d, J = 8.2 Hz, 1H), 5.80 (s, 1H), 3.87 (s, 3H), 3.35 (t, J = 5.9 Hz, 2H), 3.09 – 2.85 (m, 2H); ^{13}C NMR (75 MHz, DMSO-d_6) δ 198.3, 163.0, 156.5, 155.9, 130.2, 130.1, 129.7, 117.7, 113.9, 105.9, 102.4, 55.5, 38.3, 24.6; HR-MS (ESI) *m/z*: calcd for $C_{16}H_{16}O_4$ $[M-H]^-$ 271.0975, found 271.0976; Purity: 99.4% (by HPLC).

*3-(2,4-Dihydroxyphenyl)-1-(m-tolyl)propan-1-one (**11b**)*. Yield 80%, yellow oil. ^{1}H NMR (300 MHz, $CDCl_3$) δ 8.27 (s, 1H), 7.78 (d, J = 9.3 Hz, 2H), 7.36 (dt, J = 14.8, 7.5 Hz, 2H), 6.96 (d, J = 8.1 Hz, 1H), 6.47 (d, J = 2.6 Hz, 1H), 6.39 (dd, J = 8.2, 2.5

Hz, 1H), 6.00 (s, 1H), 3.39 (t, *J* = 6.0 Hz, 2H), 2.96 (t, *J* = 6.0 Hz, 2H), 2.40 (s, 3H); ^{13}C NMR (75 MHz, $CDCl_3$) δ 203.0, 155.7, 155.3, 138.6, 136.2, 134.7, 131.4, 129.0, 128.6, 125.7, 120.0, 108.1, 104.5, 40.7, 23.1, 21.4; HR-MS (ESI) *m/z*: calcd for $C_{16}H_{16}O_3$ $[M-H]^-$ 255.1026, found 255.1028; Purity: 96.7% (by HPLC).

*1,3-Bis(2,4-dihydroxyphenyl)propan-1-one (**11c**).* Yield 64%, yellow oil. ^{1}H NMR (300 MHz, DMSO-d_6) δ 12.70 (s, 1H, -OH), 10.62 (s, 1H, -OH), 9.24 (s, 1H, -OH), 9.00 (s, 1H, -OH), 7.79 (d, *J* = 8.9 Hz, 1H, -Ar), 6.84 (d, *J* = 8.2 Hz, 1H, -Ar), 6.34 (dd, *J* = 8.8, 2.4 Hz, 1H, -Ar), 6.25 (dd, *J* = 9.6, 2.3 Hz, 2H, -Ar), 6.11 (dd, *J* = 8.1, 2.4 Hz, 1H, -Ar), 3.15 – 3.04 (m, 2H, -CH_2-), 2.78 – 2.66 (m, 2H, -CH_2-); ^{13}C NMR (75 MHz, DMSO-d_6) δ 205.0, 165.2, 164.8, 157.1, 156.3, 133.4, 130.6, 117.8, 112.9, 108.6, 106.4, 102.9, 92.5, 29.5, 25.4; HR-MS (ESI) *m/z*: calcd for $C_{15}H_{14}O_5$ $[M-H]^-$ 273.0768, found 273.0767; Purity: 99.7% (by HPLC).

*3-(2,4-Dihydroxyphenyl)-1-(2-hydroxyphenyl)propan-1-one (**11d**).* Yield 83%, light yellow solid. ^{1}H NMR (300 MHz, DMSO-d_6) δ 11.99 (s, 1H), 9.22 (s, 1H), 8.98 (s, 1H), 7.91 (dd, *J* = 7.7, 1.7 Hz, 1H), 7.57 – 7.47 (m, 1H), 6.95 (d, *J* = 9.1 Hz, 2H), 6.85 (d, *J* = 8.1 Hz, 1H), 6.27 (d, *J* = 2.1 Hz, 1H), 6.12 (dt, *J* = 8.3, 1.7 Hz, 1H), 3.24 (t, *J* = 7.6 Hz, 2H), 2.75 (t, *J* = 7.5 Hz, 2H); ^{13}C NMR (75 MHz, DMSO-d_6) δ 206.8, 161.2, 157.1, 156.3, 136.5, 131.2, 130.6, 120.6, 119.7, 118.1, 117.7, 106.4, 102.8, 25.0, 22.3; HR-MS (ESI) *m/z*: calcd for $C_{15}H_{14}O_4$ $[M-H]^-$ 257.0819, found 257.0818; Purity: 98.2% (by HPLC).

*1-(4-Bromophenyl)-3-(2,4-dihydroxyphenyl)propan-1-one (**11e**).* Yield 86%, pink oil. ^{1}H NMR (300 MHz, $CDCl_3$) δ 7.93 (s, 1H), 7.83 (d, *J* = 8.7 Hz, 2H), 7.59 (d, *J* =

8.1 Hz, 2H), 6.95 (d, *J* = 8.2 Hz, 1H), 6.44 – 6.37 (m, 1H), 6.34 (d, *J* = 2.5 Hz, 1H), 4.86 (s, 1H), 3.36 (t, *J* = 5.9 Hz, 2H), 2.95 (t, *J* = 6.0 Hz, 2H); ^{13}C NMR (75 MHz, DMSO-d_6) δ 199.1, 156.6, 155.8, 135.6, 131.8, 130.1, 130.0, 127.1, 117.4, 105.9, 102.4, 24.26, 20.3; HR-MS (ESI) *m/z*: calcd for $C_{15}H_{13}BrO_3$ $[M-H]^-$ 318.9975, found 318.9976; Purity: 99.2% (by HPLC).

3-(2,4-Dihydroxyphenyl)-1-(o-tolyl)propan-1-one ***(11f)***. Yield 90%, yellow oil. ^{1}H NMR (300 MHz, $CDCl_3$) δ 8.10 (d, *J* = 3.8 Hz, 1H), 7.62 (dd, *J* = 7.6, 3.6 Hz, 1H), 7.32 (dd, *J* = 7.8, 4.1 Hz, 1H), 7.19 (td, *J* = 7.5, 7.0, 3.9 Hz, 2H), 6.88 (dd, *J* = 8.2, 3.9 Hz, 1H), 6.39 (dd, *J* = 4.1, 2.5 Hz, 1H), 6.32 (dt, *J* = 8.5, 3.1 Hz, 1H), 5.35 (s, 1H), 3.35 – 3.15 (m, 2H), 2.88 (d, *J* = 6.6 Hz, 2H), 2.41 (s, 3H); ^{13}C NMR (75 MHz, DMSO-d_6) δ 204.7, 157.0, 156.3, 138.6, 137.2, 132.0, 131.5, 130.5, 128.9, 126.3, 117.9, 106.3, 102.9, 41.9, 25.0, 21.0; HR-MS (ESI) *m/z*: calcd for $C_{16}H_{16}O_3$ $[M-H]^-$ 255.1026, found 255.1025; Purity: 98.7% (by HPLC).

3-(2,4-Dihydroxyphenyl)-1-(4-hydroxyphenyl)propan-1-one ***(11g)***. Yield 67%, colorless oil. ^{1}H NMR (300 MHz, $CDCl_3$) δ 8.55 (s, 1H), 7.95 (d, *J* = 9.0 Hz, 2H), 7.26 (s, 1H), 7.02 – 6.82 (m, 3H), 6.43 (d, *J* = 2.6 Hz, 1H), 6.36 (dd, *J* = 8.2, 2.6 Hz, 1H), 5.18 (s, 1H), 3.43 – 3.25 (m, 2H), 2.99 – 2.83 (m, 2H); ^{13}C NMR (101 MHz, $CDCl_3$) δ 201.1, 164.1, 155.6, 131.3, 130.8, 129.1, 120.3, 113.8, 107.9, 104.6, 40.3, 22.9; HR-MS (ESI) *m/z*: calcd for $C_{15}H_{14}O_4$ $[M-H]^-$ 257.0819, found 257.0815; Purity: 98.1% (by HPLC).

1-(2,4-Dichlorophenyl)-3-(2,4-dihydroxyphenyl)propan-1-one ***(11h)***. Yield 48%, pink oil. ^{1}H NMR (300 MHz, $CDCl_3$) δ 7.52 – 7.39 (m, 2H), 7.33 – 7.27 (m, 1H), 6.94

(d, *J* = 8.1 Hz, 1H), 6.44 – 6.32 (m, 2H), 5.06 (s, 2H), 3.34 (t, *J* = 6.2 Hz, 2H), 2.93 (t, *J* = 6.3 Hz, 2H); ^{13}C NMR (75 MHz, $CDCl_3$) δ 203.7, 155.5, 155.1, 138.1, 136.3, 132.6, 131.3, 130.7, 130.6, 127.4, 119.4, 108.0, 104.1, 44.5, 23.3; HR-MS (ESI) *m/z*: calcd for $C_{15}H_{12}Cl_2O_3$ $[M-H]^-$ 309.0090, found 309.0094; Purity: 97.9% (by HPLC).

3-(2,4-Dihydroxyphenyl)-1-(2-hydroxy-4-methoxyphenyl)propan-1-one ***(11i)***. Yield 35%, pink solid. ^{1}H NMR (300 MHz, DMSO-d_6) δ 12.72 (s, 1H), 9.24 (s, 1H), 8.99 (s, 1H), 7.88 (d, *J* = 8.8 Hz, 1H), 6.85 (d, *J* = 8.2 Hz, 1H), 6.55 – 6.49 (m, 1H), 6.47 (d, *J* = 2.4 Hz, 1H), 6.28 (d, *J* = 2.4 Hz, 1H), 6.12 (dd, *J* = 8.1, 2.4 Hz, 1H), 3.82 (s, 3H), 3.16 (d, *J* = 7.2 Hz, 2H), 2.74 (t, *J* = 7.7 Hz, 2H); ^{13}C NMR (101 MHz, DMSO-d_6) δ 205.4, 166.0, 164.7, 157.1, 156.3, 133.0, 130.6, 117.7, 113.8, 107.7, 106.4, 102.9, 101.3, 56.2, 40.0, 25.3; HR-MS (ESI) *m/z*: calcd for $C_{16}H_{16}O_5$ $[M-H]^-$ 287.0925, found 287.0924; Purity: 99.1% (by HPLC).

3-(2,4-Dihydroxyphenyl)-1-(4-isopropylphenyl)propan-1-one ***(11j)***. Yield 82%, yellow oil. ^{1}H NMR (300 MHz, $CDCl_3$) δ 8.38 (s, 1H), 7.91 (d, *J* = 7.8 Hz, 2H), 7.29 (d, *J* = 7.8 Hz, 2H), 6.94 (d, *J* = 8.1 Hz, 1H), 6.44 (d, *J* = 2.4 Hz, 1H), 6.36 (dd, *J* = 8.2, 2.5 Hz, 1H), 5.34 (s, 1H), 3.38 (t, *J* = 5.9 Hz, 2H), 3.00 – 2.88 (m, 3H), 1.26 (s, 6H); ^{13}C NMR (75 MHz, $CDCl_3$) δ 202.3, 155.6, 155.4, 154.5, 133.9, 131.3, 128.7, 126.8, 120.2, 107.9, 104.6, 40.6, 34.3, 23.6, 22.8; HR-MS (ESI) *m/z*: calcd for $C_{18}H_{20}O_3$ $[M-H]^-$ 283.1339, found 283.1334; Purity: 98.0% (by HPLC).

3-(2,4-Dihydroxyphenyl)-1-(3-hydroxy-4-methoxyphenyl)propan-1-one ***(11k)***. Yield 52%, white solid. ^{1}H NMR (300 MHz, $CDCl_3$) δ 9.37 (s, 1H), 9.20 (s, 1H), 8.98 (s, 1H), 7.48 (dd, *J* = 8.4, 2.1 Hz, 1H), 7.35 (d, *J* = 2.2 Hz, 1H), 6.99 (d, *J* = 8.5 Hz,

1H), 6.83 (d, *J* = 8.2 Hz, 1H), 6.27 (d, *J* = 2.3 Hz, 1H), 6.11 (dd, *J* = 8.1, 2.4 Hz, 1H), 3.83 (s, 3H), 3.06 (t, *J* = 7.6 Hz, 2H), 2.69 (t, *J* = 7.7 Hz, 2H); ^{13}C NMR (101 MHz, MeOD) *δ* 200.8, 156.4, 155.8, 152.2, 146.2, 130.1, 121.5, 118.6, 114.2, 113.5, 110.3, 106.0, 102.2, 55.0, 38.6, 25.2; HR-MS (ESI) *m/z*: calcd for $C_{16}H_{16}O_5$ $[M-H]^-$ 287.0925, found 287.0926; Purity: 98.4% (by HPLC).

3-(2,4-Dihydroxyphenyl)-1-phenylpropan-1-one ***(11l)***. Yield 53%, pink solid. ^{1}H NMR (300 MHz, $CDCl_3$) *δ* 8.20 (s, 1H), 7.97 – 7.92 (m, 2H), 7.55 (t, *J* = 7.4 Hz, 1H), 7.44 (d, *J* = 7.6 Hz, 2H), 7.40 (s, 1H), 6.93 (d, *J* = 8.2 Hz, 1H), 6.44 (d, *J* = 2.5 Hz, 1H), 6.36 (dd, *J* = 8.2, 2.6 Hz, 1H), 3.38 (t, *J* = 5.9 Hz, 2H), 2.94 (t, *J* = 6.0 Hz, 2H); ^{13}C NMR (75 MHz, $CDCl_3$) *δ* 202.6, 155.7, 155.3, 136.1, 133.8, 131.3, 128.7, 128.4, 119.9, 108.0, 104.5, 40.6, 23,0; HR-MS (ESI) *m/z*: calcd for $C_{15}H_{14}O_3$ $[M-H]^-$ 241.0870, found 241.0866; Purity: 98.0% (by HPLC).

3-(2,4-Dihydroxyphenyl)-1-(4-hydroxy-3-methoxyphenyl)propan-1-one ***(11m)***. Yield 63%, pink solid. ^{1}H NMR (300 MHz, MeOD) *δ* 7.57 (d, *J* = 7.7 Hz, 2H), 6.84 (dd, *J* = 11.8, 8.1 Hz, 2H), 6.29 (d, *J* = 2.4 Hz, 1H), 6.20 (dd, *J* = 8.2, 2.4 Hz, 1H), 3.89 (s, 3H), 3.15 (t, *J* = 7.7 Hz, 2H), 2.85 (t, *J* = 7.7 Hz, 2H); ^{13}C NMR (75 MHz, MeOD) *δ* 200.7, 156.4, 155.8, 152.3, 147.7, 130.2, 128.6, 123.3, 118.6, 114.5, 110.8, 106.0, 102.1, 54.9, 38.7, 19.5; HR-MS (ESI) *m/z*: calcd for $C_{16}H_{16}O_5$ $[M-H]^-$ 287.0925, found 287.0922; Purity: 95.5% (by HPLC).

1-([1,1'-Biphenyl]-4-yl)-3-(2,4-dihydroxyphenyl)propan-1-one ***(11n)***. Yield 50%, yellow oil. ^{1}H NMR (300 MHz, DMSO-d_6) *δ* 9.27 (s, 1H), 9.03 (s, 1H), 8.03 (d, *J* = 8.3 Hz, 2H), 7.74 (dd, *J* = 20.2, 7.9 Hz, 4H), 7.44 (dt, *J* = 23.4, 7.2 Hz, 3H), 6.89 (d, *J* =

8.2 Hz, 1H), 6.44 – 6.28 (m, 1H), 6.18 (dd, *J* = 8.1, 2.5 Hz, 1H), 3.23 (t, *J* = 7.7 Hz, 2H), 2.80 (t, *J* = 7.6 Hz, 2H); ^{13}C NMR (75 MHz, DMSO-*d*$_6$) δ 199.4, 156.5, 155.8, 144.4, 138.9, 135.5, 130.2, 129.1, 128.7, 128.4, 127.0, 126.9, 117.6, 106.0, 102.4, 38.7, 24.5; HR-MS (ESI) *m/z*: calcd for $C_{21}H_{18}O_3$ $[M-H]^-$ 317.1183, found 317.1182; Purity: 97.8% (by HPLC).

12a–n. Compounds **12a–n** were synthesized according to the synthetic routes of compounds **11a–n**.

*1-(2,4-Dihydroxyphenyl)-3-(2,3-dimethoxyphenyl)propan-1-one (**12a**).* Yield 54%, white solid. ^{1}H NMR (300 MHz, $CDCl_3$) δ 12.76 (s, 1H), 7.67 (d, *J* = 8.6 Hz, 1H), 6.99 (d, *J* = 7.5 Hz, 1H), 6.82 (d, *J* = 8.1 Hz, 2H), 6.35 (s, 2H), 5.84 (s, 1H), 3.86 (d, *J* = 3.8 Hz, 6H), 3.18 (d, *J* = 8.3 Hz, 2H), 3.09 – 2.95 (m, 2H); ^{13}C NMR (75 MHz, DMSO-*d*$_6$) δ 204.2, 165.2, 164.7, 152.8, 147.1, 134.7, 133.4, 124.3, 122.0, 112.9, 111.5, 108.7, 102.9, 60.5, 56.0, 25.0, 20.7; HR-MS (ESI) *m/z*: calcd for $C_{17}H_{18}O_5$ $[M-H]^-$ 301.1081, found 301.1082; Purity: 99.8% (by HPLC).

*1-(2,4-Dihydroxyphenyl)-3-(4-hydroxyphenyl)propan-1-one (**12b**).* Yield 75%, yellow solid. ^{1}H NMR (300 MHz, DMSO-*d*$_6$) δ 12.63 (s, 1H), 10.61 (s, 1H), 9.15 (s, 1H), 7.80 (d, *J* = 8.8 Hz, 1H), 7.05 (d, *J* = 8.3 Hz, 2H), 6.69 – 6.61 (m, 2H), 6.36 (dd, *J* = 8.8, 2.4 Hz, 1H), 6.24 (d, *J* = 2.2 Hz, 1H), 3.20 (t, *J* = 7.6 Hz, 2H), 2.81 (t, *J* = 7.6 Hz, 2H); ^{13}C NMR (75 MHz, DMSO-*d*$_6$) δ 204.3, 165.2, 164.7, 156.0, 133.5, 131.5, 129.7, 115.52, 113.0, 108.6, 102.9, 34.0, 29.5; HR-MS (ESI) *m/z*: calcd for $C_{15}H_{14}O_4$ $[M-H]^-$ 257.0819, found 257.0821; Purity: 96.9% (by HPLC).

1-(2,4-Dihydroxyphenyl)-3-(2,3,4-trimethoxyphenyl)propan-1-one ***(12c)***. Yield 48%, light yellow solid. ^{1}H NMR (300 MHz, DMSO-d_6) δ 12.60 (s, 1H), 10.60 (s, 1H), 7.77 (d, J = 8.7 Hz, 1H), 6.89 (d, J = 8.5 Hz, 1H), 6.69 (d, J = 8.5 Hz, 1H), 6.37 – 6.31 (m, 1H), 6.26 – 6.20 (m, 1H), 3.77 (s, 3H), 3.73 (s, 3H), 3.71 (s, 3H), 3.14 (t, J = 7.6 Hz, 2H), 2.81 (t, J = 7.6 Hz, 2H); ^{13}C NMR (75 MHz, DMSO-d_6) δ 204.3, 165.3, 164.8, 152.5, 151.8, 142.2, 133.4, 126.7, 124.2, 112.9, 108.7, 108.2, 102.9, 61.1, 60.7, 56.2, 40.0, 25.0; HR-MS (ESI) *m/z*: calcd for $C_{18}H_{20}O_6$ $[M-H]^-$ 331.1187, found 331.1186; Purity: 96.4% (by HPLC).

1-(2,4-Dihydroxyphenyl)-3-(3-hydroxyphenyl)propan-1-one ***(12d)***. Yield 86%, light yellow solid. ^{1}H NMR (300 MHz, DMSO-d_6) δ 12.61 (s, 1H), 10.64 (s, 1H), 9.27 (s, 1H), 7.82 (d, J = 8.8 Hz, 1H), 7.07 (t, J = 7.7 Hz, 1H), 6.73 – 6.64 (m, 2H), 6.62 – 6.55 (m, 1H), 6.37 (dd, J = 8.9, 2.3 Hz, 1H), 6.26 (d, J = 2.4 Hz, 1H), 3.26 (t, J = 7.6 Hz, 2H), 2.85 (t, J = 7.5 Hz, 2H); ^{13}C NMR (75 MHz, DMSO-d_6) δ 204.0, 165.2, 164.7, 157.8, 142.9, 133.4, 129.7, 119.4, 115.8, 113.4, 113.0, 108.6, 102.9, 39.9, 30.2; HR-MS (ESI) *m/z*: calcd for $C_{15}H_{14}O_4$ $[M-H]^-$ 257.0819, found 257.0821; Purity: 99.3% (by HPLC).

1-(2,4-Dihydroxyphenyl)-3-(2-hydroxy-4-methoxyphenyl)propan-1-one ***(12e)***. Yield 62%, yellow solid. ^{1}H NMR (300 MHz, DMSO-d_6) δ 13.25–13.05 (m, 1H), 11.07 (d, J = 15.1 Hz, 1H), 9.90 (d, J = 15.4 Hz, 1H), 8.33–8.18 (m, 1H), 7.44 (d, J = 9.7 Hz, 1H), 6.89 (d, J = 3.7 Hz, 1H), 6.85–6.80 (m, 1H), 6.80–6.74 (m, 1H), 6.71 (t, J = 5.6 Hz, 1H), 3.78 (s, 3H), 3.60 (d, J = 10.0 Hz, 2H), 3.10–2.90 (m, 2H); ^{13}C NMR (75 MHz, DMSO-d_6) δ 204.8, 165.2, 164.8, 159.1, 156.4, 133.4, 130.7, 119.7, 112.9, 108.6, 104.5,

102.9, 101.7, 55.3, 40.0, 25.2; HR-MS (ESI) *m/z*: calcd for $C_{16}H_{16}O_5$ $[M-H]^-$ 287.0925, found 287.0924; Purity: 97.8% (by HPLC).

1-(2,4-Dihydroxyphenyl)-3-(3-hydroxy-4-methoxyphenyl)propan-1-one ***(12f)***. Yield 74%, white solid. ^{1}H NMR (300 MHz, DMSO-d_6) δ 12.61 (s, 1H), 8.78 (s, 1H), 7.81 (s, 1H), 6.80 (d, J = 8.2 Hz, 1H), 6.71–6.57 (m, 2H), 6.35 (d, J = 8.9 Hz, 1H), 6.24 (s, 1H), 3.72 (s, 3H), 3.19 (d, J = 7.2 Hz, 2H), 2.79 (t, J = 7.6 Hz, 2H); ^{13}C NMR (75 MHz, DMSO-d_6) δ 204.2, 165.2, 164.7, 146.8, 146.4, 134.1, 133.4, 119.2, 116.3, 113.0, 112.7, 108.6, 102.9, 56.1, 39.9, 29.6; HR-MS (ESI) *m/z*: calcd for $C_{16}H_{16}O_5$ $[M-H]^-$ 287.0925, found 287.0939; Purity: 98.7% (by HPLC).

1-(2,4-Dihydroxyphenyl)-3-(3,4,5-trimethoxyphenyl)propan-1-one ***(12g)***. Yield 67%, white solid. ^{1}H NMR (300 MHz, DMSO-d_6) δ 12.61 (s, 1H), 10.62 (s, 1H), 7.83 (d, J = 8.9 Hz, 1H), 6.58 (s, 2H), 6.36 (d, J = 8.8 Hz, 1H), 6.25 (s, 1H), 3.74 (s, 6H), 3.61 (s, 3H), 3.27 (t, 2H), 2.86 (t, J = 7.9 Hz, 2H); ^{13}C NMR (75 MHz, DMSO-d_6) δ 204.2, 165.2, 164.7, 153.2, 137.2, 136.1, 133.6, 113.0, 108.6, 106.1, 102.8, 60.4, 56.2, 39.9, 30.7; HR-MS (ESI) *m/z*: calcd for $C_{18}H_{20}O_6$ $[M-H]^-$ 331.1187, found 331.1188; Purity: 97.0% (by HPLC).

1-(2,4-Dihydroxyphenyl)-3-(3,4-dimethoxyphenyl)propan-1-one ***(12h)***. Yield 67%, light yellow solid. ^{1}H NMR (300 MHz, DMSO-d_6) δ 12.63 (s, 1H), 10.65 (s, 1H), 7.82 (d, J = 8.9 Hz, 1H), 6.87 (d, J = 10.1 Hz, 1H), 6.82 (s, 1H), 6.76 (d, J = 8.2 Hz, 1H), 6.36 (d, J = 8.8 Hz, 1H), 6.30–6.16 (m, 1H), 3.73 (s, 3H), 3.70 (s, 3H), 3.29–3.22 (t, 2H), 2.86 (t, J = 7.6 Hz, 2H); ^{13}C NMR (75 MHz, DMSO-d_6) δ 204.3, 165.2, 164.7, 149.1, 147.6, 133.9, 133.5, 120.6, 113.0, 112.8, 112.3, 108.6, 102.9, 56.0, 55.8, 39.95,

30.0; HR-MS (ESI) *m/z*: calcd for $C_{17}H_{18}O_5$ $[M-H]^-$ 301.1081, found 301.1085; Purity: 98.2% (by HPLC).

*1-(2,4-Dihydroxyphenyl)-3-(3-nitrophenyl)propan-1-one (**12i**).* Yield 60%, light yellow solid. ^{1}H NMR (300 MHz, DMSO-d_6) δ 12.49 (s, 1H), 10.66 (s, 1H), 8.19 (s, 1H), 8.14–8.03 (m, 1H), 7.84 (d, J = 8.9 Hz, 1H), 7.78 (d, J = 7.7 Hz, 1H), 7.59 (t, J = 7.9 Hz, 1H), 6.36 (dd, J = 9.0, 2.3 Hz, 1H), 6.25 (d, J = 2.3 Hz, 1H), 3.42–3.34 (m, 2H), 3.07 (t, J = 7.4 Hz, 2H); ^{13}C NMR (75 MHz, DMSO-d_6) δ 203.4, 165.2, 164.5, 148.2, 144.0, 136.0, 133.5, 130.1, 123.6, 121.5, 113.0, 108.6, 102.8, 39.9, 29.5; HR-MS (ESI) *m/z*: calcd for $C_{15}H_{13}NO_5$ $[M-H]^-$ 286.0721, found 286.0720; Purity: 98.2% (by HPLC).

*1-(2,4-Dihydroxyphenyl)-3-(2-hydroxyphenyl)propan-1-one (**12j**).* Yield 56%, yellow solid. ^{1}H NMR (300 MHz, DMSO-d_6) δ 12.65 (s, 1H), 10.63 (s, 1H), 9.42 (s, 1H), 7.88–7.76 (m, 1H), 7.10 (d, J = 7.5 Hz, 1H), 6.99 (d, J = 8.0 Hz, 1H), 6.78 (d, J = 7.7 Hz, 1H), 6.71 (d, J = 7.8 Hz, 1H), 6.35 (d, J = 8.8 Hz, 1H), 6.29–6.18 (m, 1H), 3.17 (d, J = 7.8 Hz, 2H), 2.85 (d, J = 9.2 Hz, 2H); ^{13}C NMR (101 MHz, DMSO-d_6) δ 204.7, 165.2, 164.8, 155.6, 133.4, 130.3, 127.6, 127.4, 119.4, 115.3, 112.9, 108.6, 102.9, 38.1, 25.7; HR-MS (ESI) *m/z*: calcd for $C_{15}H_{14}O_4$ $[M-H]^-$ 257.0819, found 257.0819; Purity: 95.7% (by HPLC).

*1-(2,4-Dihydroxyphenyl)-3-(o-tolyl)propan-1-one (**12k**).* Yield 88%, light yellow solid. ^{1}H NMR (300 MHz, DMSO-d_6) δ 12.60 (s, 1H), 10.62 (s, 1H), 7.82 (d, J = 8.8 Hz, 1H), 7.19 (d, J = 6.2 Hz, 2H), 7.14–7.08 (m, 2H), 6.39–6.32 (m, 1H), 6.28–6.22 (m, 1H), 3.23 (t, J = 7.8 Hz, 2H), 2.90 (t, J = 7.7 Hz, 2H), 2.29 (s, 3H); ^{13}C NMR (101 MHz, DMSO-d_6) δ 204.1, 165.3, 164.7, 139.6, 136.2, 133.5, 133.5, 130.4, 129.0, 126.4, 113.0,

108.6, 102.9, 38.2, 27.6, 19.4; HR-MS (ESI) *m/z*: calcd for $C_{16}H_{16}O_3$ $[M-H]^-$ 255.1026, found 255.1029; Purity: 96.6% (by HPLC).

1-(2,4-Dihydroxyphenyl)-3-(3-methoxyphenyl)propan-1-one ***(12l)***. Yield 82%, light yellow solid. ^{1}H NMR (300 MHz, DMSO-d_6) δ 12.59 (d, J = 9.8 Hz, 1H), 10.64 (d, J = 10.0 Hz, 1H), 7.82 (t, J = 9.7 Hz, 1H), 7.18 (d, J = 9.9 Hz, 1H), 6.84 (d, J = 10.0 Hz, 2H), 6.75 (d, J = 11.3 Hz, 1H), 6.33 (d, J = 9.7 Hz, 1H), 6.27–6.18 (m, 1H), 3.73 (s, 3H), 3.30–3.19 (m, 2H), 2.88 (d, J = 9.3 Hz, 2H); ^{13}C NMR (75 MHz, $CDCl_3$) δ 203.8, 165.1, 163.1, 159.6, 142.5, 132.3, 129.7, 120.9, 114.3, 113.6, 111.6, 108.1, 103.6, 55.3, 39.6, 30.4; HR-MS (ESI) *m/z*: calcd for $C_{16}H_{16}O_4$ $[M-H]^-$ 271.0976, found 271.0978; Purity: 98.8% (by HPLC).

1-(2,4-Dihydroxyphenyl)-3-(3,4-dihydroxyphenyl)propan-1-one ***(12m)***. Yield 63%, yellow solid. ^{1}H NMR (300 MHz, DMSO-d_6) δ 12.68 (s, 1H), 10.67 (s, 1H), 8.75 (s, 1H), 7.82 (d, J = 8.8 Hz, 1H), 7.31–7.09 (m, 1H), 6.68–6.62 (m, 2H), 6.55–6.48 (m, 1H), 6.39 (dd, J = 8.9, 2.4 Hz, 1H), 6.28 (d, J = 2.4 Hz, 1H), 3.21 (t, J = 7.6 Hz, 2H), 2.78 (t, J = 7.6 Hz, 2H); ^{13}C NMR (75 MHz, DMSO-d_6) δ 204.0, 165.1, 164.5, 145.2, 143.5, 133.1, 132.0, 119.1, 116.0, 115.6, 112.6, 108.4, 102.6, 39.4, 29.4; HR-MS (ESI) *m/z*: calcd for $C_{15}H_{14}O_5$ $[M-H]^-$ 273.0768, found 273.0776; Purity: 99.9% (by HPLC).

1-(2,4-Dihydroxyphenyl)-3-(2,4-dimethoxyphenyl)propan-1-one ***(12n)***. Yield 77%, yellow oil. ^{1}H NMR (300 MHz, $CDCl_3$) δ 7.80 (d, J = 8.4 Hz, 1H), 7.38 (d, J = 3.7 Hz, 1H), 7.35 (s, 1H), 6.89 (d, J = 8.2 Hz, 1H), 6.54 (d, J = 2.2 Hz, 1H), 6.51 (dd, J = 8.4, 2.2 Hz, 1H), 6.44 (d, J = 2.4 Hz, 1H), 6.37 (dd, J = 8.2, 2.5 Hz, 1H), 3.83 (s, 3H), 3.72 (s, 3H), 3.33–3.26 (t, 2H), 2.97–2.90 (t, 2H); ^{13}C NMR (75 MHz, DMSO-d_6)

δ 204.2, 164.8, 164.4, 159.2, 158.0, 132.9, 130.0, 120.8, 112.5, 108.2, 104.4, 102.5, 98.3, 55.3, 55.1, 37.9, 24.7; HR-MS (ESI) *m/z*: calcd for $C_{17}H_{18}O_5$ $[M-H]^-$ 301.1081, found 301.1104; Purity: 98.5% (by HPLC).

13a–e. Compounds **13a–e** were synthesized according to the synthetic routes of compounds **11a–n**.

*3-(2,4-Dimethoxyphenyl)-1-(4-methoxyphenyl)propan-1-one (**13a**).* Yield 72%, pink oil. ^{1}H NMR (300 MHz, $CDCl_3$) δ 7.98 (d, J = 8.9 Hz, 2H), 7.12 (d, J = 8.1 Hz, 1H), 6.94 (d, J = 8.9 Hz, 2H), 6.48 (d, J = 2.4 Hz, 1H), 6.44 (dd, J = 8.1, 2.4 Hz, 1H), 3.88 (s, 3H), 3.83 (s, 3H), 3.81 (s, 3H), 3.23 – 3.15 (m, 2H), 3.02 – 2.94 (m, 2H); ^{13}C NMR (75 MHz, DMSO) δ 197.9, 163.0, 159.1, 158.0, 130.2, 129.9, 129.6, 121.1, 113.9, 104.3, 98.3, 55.5, 55.3, 55.1, 38.1, 24.4; HR-MS (ESI) *m/z*: calcd for $C_{18}H_{20}O_4$ $[M+H]^+$ 301.1435, found 301.1439; Purity: 99.2% (by HPLC).

*1-(2-Hydroxy-4-methoxyphenyl)-3-(2-hydroxyphenyl)propan-1-one (**13b**).* Yield 69%, white solid. ^{1}H NMR (300 MHz, $CDCl_3$) δ 7.66 (dd, J = 8.4, 0.9 Hz, 1H), 7.14–7.10 (m, 2H), 6.89 (s, 1H), 6.86 (d, J = 1.0 Hz, 1H), 6.40 (s, 2H), 3.82 (s, 3H), 3.39–3.34 (m, 2H), 3.02 (t, J = 6.3 Hz, 2H); ^{13}C NMR (75 MHz, $CDCl_3$) δ 204.8, 166.5, 165.4, 154.3, 131.8, 130.6, 128.0, 127.5, 120.8, 116.9, 113.2, 108.2, 100.9, 55.6, 39.3, 25.0; HR-MS (ESI) *m/z*: calcd for $C_{16}H_{16}O_4$ $[M-H]^-$ 271.0976, found 271.0968; Purity: 96.5% (by HPLC).

*3-(2-Hydroxyphenyl)-1-(4-methoxyphenyl)propan-1-one (**13c**).* Yield 76%, colorless oil. ^{1}H NMR (300 MHz, $CDCl_3$) δ 8.44 (s, 1H), 8.01 (d, J = 8.9 Hz, 2H), 7.18–7.12 (m, 2H), 6.99–6.93 (m, 3H), 6.91 (dd, J = 7.3, 1.3 Hz, 1H), 3.91 (s, 3H), 3.49–3.42

(m, 2H), 3.10–3.04 (m, 2H); ^{13}C NMR (75 MHz, $CDCl_3$) δ 200.6, 164.1, 154.7, 130.7, 130.6, 129.1, 128.0, 128.0, 120.6, 117.5, 113.8, 55.5, 40.1, 25.0; HR-MS (ESI) *m/z*: calcd for $C_{16}H_{16}O_3$ $[M-H]^-$ 255.1026, found 255.1023; Purity: 99.7% (by HPLC).

*1-(2-Hydroxy-4-methoxyphenyl)-3-(4-hydroxyphenyl)propan-1-one (**13d**).* Yield 57%, yellow solid. ^{1}H NMR (300 MHz, $CDCl_3$) δ 12.85 (s, 1H), 7.63 (d, J = 9.6 Hz, 1H), 7.10 (d, J = 8.4 Hz, 2H), 6.77 (d, J = 8.4 Hz, 2H), 6.45–6.33 (m, 2H), 3.83 (s, 3H), 3.24–3.14 (m, 2H), 3.02–2.91 (m, 2H); ^{13}C NMR (101 MHz, $CDCl_3$) δ 204.0, 166.1, 165.3, 154.2, 132.8, 131.6, 129.5, 115.5, 113.4, 107.8, 101.0, 55.6, 40.0, 29.6; HR-MS (ESI) *m/z*: calcd for $C_{16}H_{16}O_4$ $[M-H]^-$ 271.0976, found 271.0977; Purity: 99.7% (by HPLC).

*3-(4-Hydroxyphenyl)-1-(4-methoxyphenyl)propan-1-one (**13e**).* Yield 79%, yellow solid. ^{1}H NMR (300 MHz, $CDCl_3$) δ 7.98 (d, J = 8.9 Hz, 2H), 7.14 (d, J = 6.3 Hz, 2H), 6.96 (d, J = 9.0 Hz, 2H), 6.82 (d, J = 8.5 Hz, 2H), 3.90 (s, 3H), 3.26 (t, J = 7.7 Hz, 2H), 3.02 (t, J = 7.6 Hz, 2H); ^{13}C NMR (101 MHz, $CDCl_3$) δ 199.5, 163.7, 154.5, 132.8, 130.6, 129.8, 129.5, 115.6, 113.9, 55.5, 40.5, 29.7; HR-MS (ESI) *m/z*: calcd for $C_{16}H_{16}O_3$ $[M-H]^-$ 255.1026, found 255.1022; Purity: 98.6% (by HPLC).

Mushroom TYR inhibitory activity of tested compounds. We analyzed the mTYR inhibitory activity of target compounds based on methods reported in the literature[59] with minor modifications. Compounds were dissolved in DMSO, prepared as a 10 mM stock solution, and diluted to the desired concentration with 1×PBS at pH 6.8 (8 concentration gradients were set for each compound). mTYR lyophilized powder and substrates (L-Dopa and L-Tyrosine) were each dissolved in PBS to prepare 300

U/mL mTYR solution and 2 mM L-Dopa solution or 1 mM L-Tyrosine solution. The total reaction volume was 200 μL. 80 μL of PBS, 20 μL of sample, and 60 μL of mTYR solution were added to a 96-well plate, pre-incubated at 37 ℃ for 20 min, and then 40 μL of substrate solution was added to it and pre-incubated at 37 ℃ for 5 min (L-Dopa) or 10 min (L-Tyrosine). Afterwards, absorbance at 490 nm was measured immediately with a microplate reader, PBS solvent used as blank control, and measured three times in parallel.

mTYR inhibitory mechanism study of 11c and 11m. Under different concentrations of L-Tyrosine (0.4 mM, 0.35 mM, 0.3 mM, 0.25 mM, 0.2 mM, 0.15 mM, 0.1 mM, 0.05 mM) and **11c** or **11m** (0 mM, 0.025 mM, 0.05 mM, 0.1 mM), the enzyme inhibition types of the compounds were analyzed and measured four times in parallel. The method was the same as that of IC_{50}. The inhibition type of the compounds on the enzyme was determined by using the Lineweaver-Burk double reciprocal diagram ($1/V = K_m/V_{max}\ 1/([S]) + 1/V_{max}$) with different concentrations of L-Tyrosine.

Molecular docking. The X-ray crystal structure (PDB ID: 2Y9X) of mTYR from *Agaricus bisporus* was downloaded from the protein database. The protein was then prepared through the Protein Preparation Wizard module in Schrödinger, and compounds **11c** and **11m** were prepared by the Ligprep module. Their force fields were then minimized by OPLS-2005. Finally, Glide Extra Precision (Glide-XP) in Ligand Docking module was used for extra precision docking of compounds with proteins, and PyMOL Molecular Graphics System version 2.7 was used to process docking images.

Antioxidant activity of representative compounds 11a–n. Representative compounds were tested for their DPPH free radical scavenging activity using methods reported in the literature[60,61] with some modifications. In a 96-well plate, 180 μL of DPPH in methanol (0.2 mM) was mixed with 20 μL of a representative compound in DMSO (0.5 mM). L-ascorbic acid was used as standard reference material, and 20 μL of DMSO was added to the blank group. The 96-well plate was then incubated in the dark for 1 h. Absorbance was measured at 517 nm using a microplate reader and all experiments were repeated three times in parallel. The DPPH radical scavenging activity of representative compounds was calculated using the following formula: % radical scavenging rate = [(Ac-As)/Ac] × 100. Ac refers to the absorbance of the blank group, and As refers to the absorbance of the test group.

Cytotoxicity of 11c and 11m. B16F10 and A375 cells were used for determination of the cytotoxicity of representative compounds **11c** and **11m**. The cells were cultured in DMEM high glucose medium containing 10% fetal bovine serum. The cells in logarithmic growth phase were digested, counted, suspended, and seeded into 96-well plates at a rate of 3×10^3 cells/well. After 24 h of culture, the compound solutions were added to the culture to make final concentrations of the compound at 5 μM, 10 μM and 50 μM for cell B16F10; 50 μM for cell A375. After incubatation at 37 ℃ in 5% CO_2 for 72 h, 20 μL of 5 mg/L MTT was then added to the culture. After incubation in the incubator for 4 days, the culture medium was sucked away, and methylzan was dissolved with 150 μL DMSO. The absorbance at 490 nm was measured with a microplate reader.

TYR inhibitory activity of 11c and 11m. The B16F10 and A375 cells in the logarithmic growth phase were digested, resuspended, and counted, then seeded into 24-well plates at a rate of 3×10^4 cells/well, and incubated at 37 ℃ in a 5% CO_2 incubator for 24 h. 1 μM α-MSH was added to the blank control group, positive control group and experimental groups. For cells B16F10, the positive control group was treated with 25 μM kojic acid and the experimental groups were treated with 5, 10, and 25 μM **11c** or **11m** respectively. For cells A375, the positive control group was treated with 20 μM kojic acid and the experimental groups were treated with 20 μM **11c** and **11m.** The blank group was added with DMSO (< 0.3%). After 24 h of incubation, the cells were collected into centrifuge tubes, washed twice with 1 mL of PBS, and 100 μM of 1% TritonX-100 (with 50 mM PBS, pH 6.8) containing 0.1 mM PMSF was added to lyse cells. After incubation at -80 ℃ for 30 min, it was thawed at room temperature, then centrifuged at -4 ℃ at 12×10^3 rpm for 15 min. 80 μL of the supernatant was taken out and added to a 96-well plate, and then 20 μL of bottom was added to the 96-well plate. The substance L-Dopa (2 mM) was transferred to 37 ℃ to react for 1 h, and its absorbance at 490 nm was measured with a microplate reader every 10 min. The experiment was repeated three times in parallel. % TYR activity = $OD_{\text{experimental group}}/OD_{\text{control group}} \times 100\%$.

Inhibition of 11c and 11m on melanin content. The B16F10 cells and A375 cells in the logarithmic growth phase were digested, resuspended, and counted, then seeded into 24-well plates at a rate of 3×10^4 cells/well, and incubated at 37 ℃ in a 5% CO_2 incubator for 24 h. 1 μM α-MSH was added to the blank control group, positive control

group, and experimental groups. For cells B16F10, the positive control group was treated with 25 μM kojic acid and the experimental groups were treated with 5, 10, and 25 μM **11c** and **11m**, respectively. For cells A375, the positive control group was treated with 20 μM kojic acid and the experimental groups were treated with 20 μM **11c** or **11m.** The blank group was added with DMSO (< 0.3%). After incubating in the incubator for 24 h, the cells were collected into centrifuge tubes, washed twice with 1 mL PBS, and then 100 μL of 1 M NaOH was added. They were then incubated at 60 ℃ for 1 h, and the supernatant was taken into a 96-well plate. The absorbance at 405 nm was measured with a microplate reader. The experiment was repeated three times in parallel. % Melanin content=$OD_{experimental\ group}/OD_{control\ group} \times 100\%$.

Western blotting. B16F10 cells (2×10^5 cells/well) were cultured in DMEM medium with 10% FBS and 1% penicillin/streptomycin (*v*/*v*) for 24 h and then incubated with various concentrations of compounds or DMSO for 72 h in six-well plates. Then, the cells were washed twice with ice-cold PBS and subsequently scraped in RIPA lysis buffer (Beyotime, China). The cell pellets were lysed on ice for 30 min, followed by centrifugation at 4 ℃ for another 30 min (13, 000 rpm/min) and the supernatant was quantified with BCA kit (Beyotime, China). The western blot operation process has been written in great detail in previous research. The specific primary antibodies used included those for TYR (1:1000, Abcam, Cambs, UK), MiTF (1:1000; Cell Signaling Technology, Beverly, MA), and GAPDH (1:10000; Proteintech, Wuhan, China). The secondary antibody was HRP-conjugated goat anti-rabbit-IgG (1:10000; Biosharp Beijing, China). Immunoreactive bands were visualized by enhanced

chemiluminescence using ECL plus (FUDE biology technology, Hangzhou, China) and Bio-Rad Versadoc (Tanon, Shanghai, China).

HPLC analysis of 11c and kojic acid in skin permeation study. Hypersil BDS C18 Columns, 150 mm L x 4.6 mm ID, 3.0 μm, were used as chromatographic column. The system operated at a flow rate of 0.5 mL/min. Injection volume was 10.00 μL. Column temperature was kept at 30 ℃ and UV detection at λ max = 280 nm with an emission wavelength setting. The run time for each sample was 20.00 min. The mobile phase was composed of 0.1 M acetate buffer (pH 4.0) and methanol in a ratio of 95:5 (*v*/*v*) for kojic acid and 40:60 (*v*/*v*) for **11c**.

Linearity, limit of detection and limit of quantitation. The linearity of the method was assessed over a range of concentrations. Thirteen different concentrations between 0.05 and 512 μg/mL were chosen for **11c** and kojic acid. The calibration curves were obtained by plotting the peak areas against the corresponding concentrations of **11c** or kojic acid. The slope, y-intercept, and correlation co-efficient (R^2) of the curve were determined by linear regression analysis. According to FDA regulations[62], the theoretical LOD and LOQ for the developed method were calculated using standard deviation of the response (σ) and slope (S) of the calibration curve according to the following equations:

$LOD = 3.3\sigma/S$, $LOQ = 10\sigma/S$

The equation for the relationship between concentration and area was obtained as $y=1.6456x-0.0178$, where the coefficient of determination was 0.9998. Meanwhile, the calibration curve for kojic acid standard was obtained as, $y=1.1165x+0.0091$, and the

regression coefficient was 0.9999. This indicates that the curves are accurate and the regression effect is more significant and credible. The detection limit of **11c** was 0.1323 μg/mL, and the limit of quantification was 0.4010 μg/mL. The detection limit of kojic acid was 0.1448 μg/mL and the limit of quantification was 0.4388 μg/mL.

***In vitro* skin permeation efficiency of 11c and kojic acid by Franz cell components.** Skin samples were prepared from 6-month-old pigs obtained from local abattoirs and then steamed cleaned. The skin was kept at 4 ℃ for a maximum of no more than 24 hours, the tissue was washed with ultrapure water only, and the hair was trimmed with scissors. Excess subcutaneous fat was removed and the skin was wrapped in aluminium foil and stored in the fridge at -20 ℃ for a maximum of 3 months. The entire thickness of the skin was used for the Franz cell penetration experiments to prevent alteration of the biomechanical properties of the skin.

Franz cell set-up. Prior to infiltration studies, skin samples were thawed at room temperature for at least 1 h. Afterwards, circular skin samples were cut and mounted between the donor and recipient compartments of the Franz-type static diffusion cell device[63], with the dermal side facing downwards, an exposed surface area of 0.64 cm^2, and a recipient compartment volume of 3 mL. The trimmed skin samples were placed over the recipient compartment for 15 min to allow equilibration prior to skin treatment. The integrity of each skin sample was assessed by resistance using the method and guidelines described by Davies et al., 2004[64], and only skin that yielded resistance readings greater than 10 kΩ was used. PBS solution (pH 7.4) was used as the recipient medium. 200 mL of 2 mg/mL of **11c** or kojic acid in PG was administered through the

donor chamber, and 200 mL of distilled water was used as a control. The water bath temperature at 36.5℃ was maintained throughout the experiment. The skin was exposed to the compound preparation for various time points of 0.5, 1, 2, 4, and 24 h. Each preparation was run 3 times at each time point to ensure accuracy.

Post Franz cell skin tissue preparation. After the permeation experiments, the excess liquid was removed and collected from the skin surface by careful application of sponges soaked with 3% *v*/*v* Teepol solution. The sponges were pooled for HPLC analysis as a total skin wash. Any formulation which might have spread to the donor chamber was collected by the sponges and stored for HPLC analysis as a donor chamber wash. Upon removing the excess formulation from the skin surface, 15 sequential tape strips were collected from the skin as tape strips. The amount of **11c** from the different Franz cell components (skin wash, donor chamber wash, pooled tape strips, and remaining within skin after tape stripping) were extracted by the addition of 5, 5, 10, and 5 mL of methanol extraction mixture (methanol 30%: water) respectively. Samples were then vortexed for 1 min and sonicated for 30 min. The extracts (1 mL) were then collected. For the receptor fluid, 1 mL of the solution from each Franz cell was collected. All the samples were centrifuged at 4 ℃ at 14000 rpm for 10 min and then filtered through the 0.22 μm membrane.

Visualization of 11c within the skin by OrbiSIMS. The 2 h skin samples were chosen from the Franz cell permeation test and the surface of the skin was scrubbed with a sponge moistened with distilled water to remove excess formulation. The skin was then scrubbed with a dry sponge. The skin samples were then immediately frozen

using liquid nitrogen to avoid morphological distortion and tissue damage caused by autolysis or decay. The skin samples were then placed on a Cryostat (Leica Biosystems, Wetzlar, Germany) for frozen sectioning (CT -24 ℃, OT -30 ℃), and 20 μm thick transverse skin sections were cut, with three sections per sample being placed on the slide. For each sample, adjacent 20 μm thick sections were used for standard hematoxylin-eosin staining controls.

3D OrbiSIMS imaging analysis. For permeation analysis, skin cross-sections were used. A 3D OrbiSIMS (Hybrid SIMS, IONTOF GmbH, Germany) analysis was performed on a hybrid instrument (IONTOF GmbH). For the Orbitrap image acquisition, a 20 KeV Ar3000+ analysis beam with a diameter of 20 μm was used as the primary ion source. Samples were analyzed at room temperature across a 300 × 300 μm area in negative polarity. Ar3000+ primary ions were used with a filament current of 2.30A with charge compensation performed using a low-energy (-20 eV) electron flood gun. Duty cycle was set to 4.4% and cycle time to 200 μs. Argon gas flooding was in operation to aid with charge compensation, which led to a pressure of 9.0×10^{-7} mbar in the main chamber. The optimal target surface potential was at 136.6 V. Mass spectra were recorded at a resolution of 240,000 at *m*/*z* 200 in the mass range of 75 to 1,125 *m*/*z*. The automatic gain control (AGC) target was off with the maximum injection time set at 500 ms. Both data acquisition and the subsequent data processing were performed using SurfaceLab 7 software (IONTOF GmbH). Orbitrap data were acquired using a Thermo Fisher Orbitrap HF mass spectrometer.

In vivo **treatment of 11c on UV-induced skin pigmentation.** The animal experiments were performed using the previously reported method[44] with minor modifications. All the experiments were conducted on the basis of the approval and guidelines of the Ethics Review Committee of China Pharmaceutical University (animal experiment ethical review acceptance No. 2022-06-012), as well as the Animal Welfare Act and principles stated in the Guide for the Care and Use of Laboratory Animals of the National Research Council. Female guinea pigs (Dunkin−Hartley strain, 10 weeks old, 350−500 g, Nanjing, China) were used as experimental subjects. On the backs of the guinea pigs, four separate areas (2 × 2 cm^2) were shaved and received ultraviolet exposure from a UV lamp (SH1-B, Sigma, Shanghai, China), with a total UV dose of 30 mJ/cm^2/day. Each separate area was treated with different formulations with or without different doses of the compound. The effect of the compound was examined on the basis of a pigmentation model with two different methods of administration: topical administration of the compound 1) 6 h before UV radiation every day for 2 weeks, or 2) after exposure to UV lamp for 5 days/week for two consecutive weeks. Three days after the final operation, the animals in both groups were sacrificed and skin samples were removed surgically. The skin samples were sent to KeyGEN Biotechnology Company (Nanjing, China) for tissue sectioning, staining, and photographing. Melanin content was assessed using a Fontana−Masson Stain Kit (Solarbio, Beijing, China) following the manufacturer's instruction. The proportion of the positive cells was the ratio of the number of positive cells to the number of epidermal cells in the same visual field with 10 different images for each skin sample.

ASSOCIATED CONTENT

Supporting Information

The Supporting Information is available free of charge on the ACS Publications website at DOI:

^{1}H and ^{13}C NMR spectra, HRMS spectra and HPLC spectrograms for all target compounds (PDF);

SMILES molecular formula strings (CSV);

mTYR bound with compound **11c** and **11m** (PDB).

AUTHOR INFORMATION

Corresponding Authors

*E-mail: david.scurr@nottingham.ac.uk (D. Scurr)

*E-mail: Zheying.Zhu@nottingham.ac.uk (Z. Zhu)

*E-mail: jinyixu@china.com (J. Xu)

*E-mail: cpuxst@163.com (S. Xu)

ORCID

Shengtao Xu: 0000-0002-5705-6377

Jinyi Xu: 0000-0002-1961-0402

Zheying Zhu: 0000-0002-2135-3812

David Scurr: 0000-0003-0859-3886

Author Contributions

The manuscript was written through contributions of all authors. All authors have given approval to the final version of the manuscript.

[#]Songtao Xue and Zhiwei Li contributed equally to this study.

Notes

The authors declare no competing financial interest.

ACKNOWLEDGMENTS

This study was supported from the National Natural Science Foundation of China (No. 81973167, 82173672, and 82173679) and "Double First-Class" University project of China Pharmaceutical University (CPUQNJC22).

ABBREVIATIONS USED

3D OrbiSIMS, 3D orbitrap secondary ion mass spectrometry; CP, carbomer; DPPH, 2,2-diphenyl-1-picrylhydrazyl; EB, Epidermis basal layer; HPLC, high performance liquid chromatography; MiTF, melanocyte inducing transcription factor; MTT, 3-(4,5-dimethylthiazol-2-yl)-2,5-diphenyltetrazolium bromide; mTYR, mushroom tyrosinase;

PG, propylene glycol; TYR, tyrosinase; TYRP-1, tyrosine-related protein 1; TYRP-2, tyrosine-related protein 2; UVR, ultraviolet radiation; α-MSH, α-melanocyte stimulating hormone.

REFERENCES

(1) Nicolaidou, E.; Katsambas, A. D. Pigmentation disorders: hyperpigmentation and hypopigmentation. *Clin. Dermatol.* **2014**, *32*, 66–72.

(2) Yamaguchi, Y.; Hearing, V. J. Physiological factors that regulate skin pigmentation. *Biofactors* **2009**, *35*, 193–199.

(3) Ünver, N.; Freyschmidt-Paul, P.; Hörster, S.; Wenck, H.; Stäb, F.; Blatt, T.; Elsässer, H. P. Alterations in the epidermal-dermal melanin axis and factor XIIIa melanophages in senile lentigo and ageing skin: melanophages in the dermis of senile lentigo and ageing Skin. *Br. J. Dermatol.* **2006**, *155*, 119–128.

(4) Li, G.; Ju, H. K.; Chang, H. W.; Jahng, Y.; Lee, S. H.; Son, J. K. Melanin biosynthesis inhibitors from the bark of machilus thunbergii. *Biol. Pharm. Bull.* **2003**, *26*, 1039–1041.

(5) Iozumi, K.; Hoganson, G. E.; Pennella, R.; Everett, M. A.; Fuller, B. B. Role of tyrosinase as the determinant of pigmentation in cultured human melanocytes. *J. Invest. Dermatol.* **1993**, *100*, 806–811.

(6) Ahn, S. J.; Koketsu, M.; Ishihara, H.; Lee, S. M.; Ha, S. K.; Lee, K. H.; Kang, T. H.; Kima, S. Y. Regulation of melanin synthesis by selenium-containing carbohydrates. *Chem. Pharm. Bull. (Tokyo)* **2006**, *54*, 281–286.

(7) Brenner, M.; Hearing, V. J. The protective role of melanin against UV damage in human skin. *Photochem. Photobiol.* **2008**, *84*, 539–549.

(8) *The pigmentary system: physiology and pathophysiology*, 1st ed.; Nordlund, J. J., Boissy, R. E., Hearing, V. J., King, R. A., Oetting, W. S., Ortonne, J., Eds.; Wiley, **2006**.

(9) Findlay, G. H. Ochronosis following skin bleaching with hydroquinone. *J. Am. Acad. Dermatol.* **1982**, *6*, 1092–1093.

(10) Hoshaw, R. A.; Zimmerman, K. G.; Menter, A. Ochronosislike pigmentation from hydroquinone bleaching creams in American blacks. *Arch. Dermatol.* **1985**, *121*, 105–108.

(11) Meys, R. Skin pigmentation. *Dermatol. Part 2 2* **2017**, *45*, 438–443.

(12) Liu-Smith, F.; Meyskens, F. L. Molecular mechanisms of flavonoids in melanin synthesis and the potential for the prevention and treatment of melanoma. *Mol. Nutr. Food Res.* **2016**, *60*, 1264–1274.

(13) Krejci, P.; Aklian, A.; Kaucka, M.; Sevcikova, E.; Prochazkova, J.; Masek, J. K.; Mikolka, P.; Pospisilova, T.; Spoustova, T.; Weis, M.; Paznekas, W. A.; Wolf, J. H.; Gutkind, J. S.; Wilcox, W. R.; Kozubik, A.; Jabs, E. W.; Bryja, V.; Salazar, L.; Vesela, I.; Balek, L. Receptor tyrosine kinases activate canonical WNT/β-catenin signaling via MAP kinase/LRP6 pathway and direct *β*-catenin phosphorylation. *PLOS ONE* **2012**, *7*, e35826.

(14) Sasaki, M.; Horikoshi, T.; Uchiwa, H.; Miyachi, Y. Up-regulation of tyrosinase gene by nitric oxide in human melanocytes. *Pigment Cell Res.* **2000**, *13*, 248–252.

(15) Pan, C.; Liu, X.; Zheng, Y.; Zhang, Z.; Li, Y.; Che, B.; Liu, G.; Zhang, L.; Dong, C.; Aisa, H. A.; Du, Z.; Yuan, Z. The mechanisms of melanogenesis inhibition by glabridin: molecular docking, PKA/MITF and MAPK/MITF pathways. *Food Sci. Hum. Wellness* **2023**, *12*, 212–222.

(16) Park, W.; Kwon, O.; Yoon, T.-J.; Chung, J. H. Anti-graying effect of the extract of pueraria thunbergiana via upregulation of CAMP/MITF-M signaling pathway. *J. Dermatol. Sci.* **2014**, *75*, 153–155.

(17) Swope, V. B.; Abdel-Malek, Z. A. MC1R: front and center in the bright side of dark eumelanin and DNA repair. *Int. J. Mol. Sci.* **2018**, *19*, 2667.

(18) Wang, N.; Hebert, D. N. Tyrosinase maturation through the mammalian secretory pathway: bringing color to life. *Pigment Cell Melanoma Res.* **2010**, *19*, 3–18.

(19) Pillaiyar, T.; Namasivayam, V.; Manickam, M.; Jung, S. H. Inhibitors of melanogenesis: an updated review. *J. Med. Chem.* **2018**, *61*, 7395–7418.

(20) Favre, E.; Daina, A.; Carrupt, P. A.; Nurisso, A. Modeling the Met form of human tyrosinase: a refined and hydrated pocket for antagonist design. *Chem. Biol. Drug Des.* **2014**, *84*, 206–215.

(21) Satooka, H.; Kubo, I. Resveratrol as a kcat type inhibitor for tyrosinase: potentiated melanogenesis Inhibitor. *Bioorg. Med. Chem.* **2012**, *20*, 1090–1099.

(22) Lee, T. H.; Seo, J. O.; Baek, S. H.; Kim, S. Y. Inhibitory effects of resveratrol on melanin synthesis in ultraviolet B-induced pigmentation in guinea pig skin. *Biomol. Ther.* **2014**, *22*, 35–40.

(23) Rigon, R. B.; Fachinetti, N.; Severino, P.; Santana, M. H. A.; Chorilli, M. Skin delivery and *in vitro* biological evaluation of trans-resveratrol-loaded solid lipid nanoparticles for skin disorder therapies. *Mol. Basel Switz.* **2016**, *21*, E116.

(24) Franco, D. C. Z.; de Carvalho, G. S. G.; Rocha, P. R.; da Silva Teixeira, R.; da Silva, A. D.; Raposo, N. R. B. Inhibitory effects of resveratrol analogs on mushroom tyrosinase activity. *Mol. Basel Switz.* **2012**, *17*, 11816–11825.

(25) Bae, S. J.; Ha, Y. M.; Kim, J. A.; Park, J. Y.; Ha, T. K.; Park, D.; Chun, P.; Park, N. H.; Moon, H. R.; Chung, H. Y. A novel synthesized tyrosinase inhibitor: *(E)*-2-((2,4-dihydroxyphenyl)diazenyl)phenyl 4-methylbenzenesulfonate as an azo-resveratrol analog. *Biosci. Biotechnol. Biochem.* **2013**, *77*, 65–72.

(26) Bae, S. J.; Ha, Y. M.; Park, Y. J.; Park, J. Y.; Song, Y. M.; Ha, T. K.; Chun, P.; Moon, H. R.; Chung, H. Y. Design, synthesis, and evaluation of *(E)*-*N*-substituted benzylidene-aniline derivatives as tyrosinase inhibitors. *Eur. J. Med. Chem.* **2012**, *57*, 383–390.

(27) Criton, M.; Le Mellay-Hamon, V. Analogues of *N*-hydroxy-*N*'-phenylthiourea and *N*-hydroxy-*N*'-phenylurea as inhibitors of tyrosinase and melanin formation. *Bioorg. Med. Chem. Lett.* **2008**, *18* (12), 3607–3610.

(28) Thanigaimalai, P.; Lee, K. C.; Sharma, V. K.; Joo, C.; Cho, W. J.; Roh, E.; Kim, Y.; Jung, S. H. Structural requirement of phenylthiourea analogs for their inhibitory activity of melanogenesis and tyrosinase. *Bioorg. Med. Chem. Lett.* **2011**, *21*, 6824–6828.

(29) Thanigaimalai, P.; Hoang, T. A. L.; Lee, K. C.; Bang, S. C.; Sharma, V. K.; Yun, C. Y.; Roh, E.; Hwang, B. Y.; Kim, Y.; Jung, S. H. Structural requirement(s) of *N*-

phenylthioureas and benzaldehyde thiosemicarbazones as inhibitors of melanogenesis in melanoma B16 Cells. *Bioorg. Med. Chem. Lett.* **2010**, *20*, 2991–2993.

(30) DuBOIS, K. P.; Erway, W. F. Studies on the mechanism of action of thiourea and related compounds; inhibition of oxidative enzymes and oxidations catalyzed by copper. *J. Biol. Chem.* **1946**, *165*, 711–721.

(31) Hall, A. M.; Orlow, S. J. Degradation of tyrosinase induced by phenylthiourea occurs following Golgi maturation. *Pigment Cell Res.* **2005**, *18*, 122–129.

(32) Poma, A.; Bianchini, S.; Miranda, M. Inhibition of L-tyrosine-induced micronuclei production by phenylthiourea in human melanoma cells. *Mutat. Res.* **1999**, *446*, 143–148.

(33) Zhao, D. Y.; Zhang, M. X.; Dong, X. W.; Hu, Y. Z.; Dai, X. Y.; Wei, X. Y.; Hider, R. C.; Zhang, J. C.; Zhou, T. Design and synthesis of novel hydroxypyridinone derivatives as potential tyrosinase inhibitors. *Bioorg. Med. Chem. Lett.* **2016**, *26*, 3103–3108.

(34) Feng, L.; Shi, N.; Cai, S.; Qiao, X.; Chu, P.; Wang, H.; Long, F.; Yang, H.; Yang, Y.; Wang, Y.; Yu, H. *De novo* molecular design of a novel octapeptide that inhibits *in vivo* melanogenesis and has great transdermal ability. *J. Med. Chem.* **2018**, *61*, 6846–6857.

(35) Tan, X.; Song, Y. H.; Park, C.; Lee, K. W.; Kim, J. Y.; Kim, D. W.; Kim, K. D.; Lee, K. W.; Curtis-Long, M. J.; Park, K. H. Highly potent tyrosinase inhibitor, neorauflavane from campylotropis hirtella and inhibitory mechanism with molecular docking. *Bioorg. Med. Chem.* **2016**, *24*, 153–159.

(36) Oyama, T.; Takahashi, S.; Yoshimori, A.; Yamamoto, T.; Sato, A.; Kamiya, T.; Abe, H.; Abe, T.; Tanuma, S. I. Discovery of a new type of scaffold for the creation of novel tyrosinase inhibitors. *Bioorg. Med. Chem.* **2016**, *24*, 4509–4515.

(37) Peralta, M. A.; Santi, M. D.; Agnese, A. M.; Cabrera, J. L.; Ortega, M. G. Flavanoids from dalea elegans: chemical reassignment and determination of kinetics parameters related to their anti-tyrosinase activity. *Phytochem. Lett.* **2014**, *10*, 260–267.

(38) Arung, E. T.; Shimizu, K.; Kondo, R. Structure-activity relationship of prenyl-substituted polyphenols from artocarpus heterophyllus as inhibitors of melanin biosynthesis in cultured melanoma cells. *Chem. Biodivers.* **2007**, *4*, 2166–2171.

(39) Arndt, K. A.; Fitzpatrick, T. B. Topical use of hydroquinone as a depigmenting agent. *JAMA* **1965**, *194*, 965–967.

(40) Boo, Y. C. Arbutin as a skin depigmenting agent with antimelanogenic and antioxidant properties. *Antioxid. Basel Switz.* **2021**, *10*, 1129.

(41) Breathnach, A. C.; Nazzaro-Porro, M.; Passi, S.; Zina, G. Azelaic acid therapy in disorders of pigmentation. *Clin. Dermatol.* **1989**, *7*, 106–119.

(42) Li, D. F.; Hu, P. P.; Liu, M. S.; Kong, X. L.; Zhang, J. C.; Hider, R. C.; Zhou, T. Design and synthesis of hydroxypyridinone-L-phenylalanine conjugates as potential tyrosinase inhibitors. *J. Agric. Food Chem.* **2013**, *61*, 6597–6603.

(43) Son, K. H.; Heo, M. Y. The evaluation of depigmenting efficacy in the skin for the development of new whitening agents in Korea. *Int. J. Cosmet. Sci.* **2013**, *35*, 9–18.

(44) Gonçalez, M. L.; Corrêa, M. A.; Chorilli, M. Skin Delivery of kojic acid-loaded nanotechnology-based drug delivery systems for the treatment of skin aging. *BioMed Res. Int.* **2013**, *2013*, 271–276.

(45) Feng, Y.; Wang, Z.; Chen, J.; Li, H.; Wang, Y.; Ren, D. F.; Lu, J. Separation, identification, and molecular docking of tyrosinase inhibitory peptides from the hydrolysates of defatted walnut (Juglans regia L.) Meal. *Food Chem.* **2021**, *353*, 129471.

(46) Xue, W.; Liu, X.; Zhao, W.; Yu, Z. Identification and molecular mechanism of novel tyrosinase inhibitory peptides from collagen. *J. Food Sci.* **2022**, *87*, 2744–2756.

(47) Yu, Q.; Fan, L.; Duan, Z. Five individual polyphenols as tyrosinase inhibitors: inhibitory activity, synergistic effect, action mechanism, and molecular docking. *Food Chem.* **2019**, *297*, 124910.

(48) Huang, C. H.; Sung, H. C.; Hsiao, C. Y.; Hu, S.; Ko, Y. S. Transdermal delivery of three vitamin C derivatives by Er:YAG and carbon dioxide laser pretreatment. *Lasers Med. Sci.* **2013**, *28*, 807–814.

(49) Rivière, C. Dihydrochalcones: occurrence in the plant kingdom, chemistry and biological activities. Studies in Natural Products Chemistry; Atta-ur-Rahman, Ed.; Elsevier, **2016**, *51*, 253–381.

(50) Takahashi, M.; Takara, K.; Toyozato, T.; Wada, K. A novel bioactive chalcone of morus australis inhibits tyrosinase activity and melanin biosynthesis in B16 melanoma cells. *J. Oleo Sci.* **2012**, *61*, 585–592.

(51) Lee, S. J.; Son, Y. H.; Lee, K. B.; Lee, J. H.; Kim, H. J.; Jeong, E. M.; Park, S. C.; Kim, I. G. 4-n-butylresorcinol enhances proteolytic degradation of tyrosinase in B16F10 melanoma Cells. *Int. J. Cosmet. Sci.* **2017**, *39*, 248–255.

(52) Ferro, S.; Deri, B.; Germano, M. P.; Gitto, R.; Ielo, L.; Buemi, M. R.; Certo, G.; Vittorio, S.; Rapisarda, A.; Pazy, Y.; Fishman, A.; Luca, L. D. Targeting tyrosinase: development and structural insights of novel inhibitors bearing arylpiperidine and arylpiperazine fragments. *J. Med. Chem.* **2018**, *61*, 3908-3917.

(53) Ullah, S.; Kang, D.; Lee, S.; Ikram, M.; Park, C.; Park, Y.; Yoon, S.; Chun, P.; Moon, H. R. Synthesis of cinnamic amide derivatives and their anti-melanogenic effect in α-MSH-stimulated B16F10 melanoma cells. *Eur. J. Med. Chem.* **2019**, *161*, 78–92.

(54) Sy, S.; Vk, S.; N, S. Mushroom tyrosinase: recent prospects. *J. Agric. Food Chem.* **2003**, *51*, 2837–2853.

(55) Ashooriha, M.; Khoshneviszadeh, M.; Khoshneviszadeh, M.; Rafiei, A.; Kardan, M.; Yazdian-Robati, R.; Emami, S. Kojic acid–natural product conjugates as mushroom tyrosinase inhibitors. *Eur. J. Med. Chem.* **2020**, *201*, 112480.

(56) Goding, C. R. MiTF from neural crest to melanoma: signal transduction and transcription in the melanocyte lineage. *Genes Dev.* **2000**, *14*, 1712–1728.

(57) Starr, N. J.; Khan, M. H.; Edney, M. K.; Trindade, G. F.; Kern, S.; Pirkl, A.; Kleine-Boymann, M.; Elms, C.; O'Mahony, M. M.; Bell, M.; Alexander, M. R.; Scurr, D. J. Elucidating the molecular landscape of the stratum corneum. *Proc. Natl. Acad. Sci.* **2022**, *119*, e2114380119.

(58) Kotowska, A. M.; Trindade, G. F.; Mendes, P. M.; Williams, P. M.; Aylott, J. W.; Shard, A. G.; Alexander, M. R.; Scurr, D. J. Protein identification by 3D OrbiSIMS to facilitate *in situ* imaging and depth profiling. *Nat. Commun.* **2020**, *11*, 5832.

(59) Romagnoli, R.; Baraldi, P. G.; Brancale, A.; Ricci, A.; Hamel, E.; Bortolozzi, R.; Basso, G.; Viola, G. Convergent synthesis and biological evaluation of 2-amino-4-(3',4',5'-trimethoxyphenyl)-5-aryl thiazoles as microtubule targeting agents. *J. Med. Chem.* **2011**, *54*, 5144–5153.

(60) Hong, Y.; Zhao, Y.; Yang, L.; Gao, M.; Li, L.; Man, S.; Wang, Z.; Guan, Q.; Bao, K.; Zuo, D.; Wu, Y.; Zhang, W. Design, synthesis and biological evaluation of 3,4-diaryl-1,2,5-oxadiazole-2/5-oxides as highly potent inhibitors of tubulin polymerization. *Eur. J. Med. Chem.* **2019**, *178*, 287–296.

(61) Matos, M. J.; Varela, C.; Vilar, S.; Hripcsak, G.; Borges, F.; Santana, L.; Uriarte, E.; Fais, A.; Di Petrillo, A.; Pintus, F.; Era, B. Design and discovery of tyrosinase inhibitors based on a coumarin scaffold. *RSC Adv.* **2015**, *5*, 94227–94235.

(62) Analytical Procedures and Methods Validation for Drugs and Biologics. U.S. Food and Drug Administration, **2020**.

(63) Franz, T. J. Percutaneous absorption on the relevance of *in vitro* data. *J. Invest. Dermatol.* **1975**, *64*, 190–195.

(64) Davies, D. J.; Ward, R. J.; Heylings, J. R. Multi-species assessment of electrical resistance as a skin integrity marker for *in vitro* percutaneous absorption studies. *Toxicol. In Vitro* **2004**, *18*, 351–358.

Table of Contents Graphic